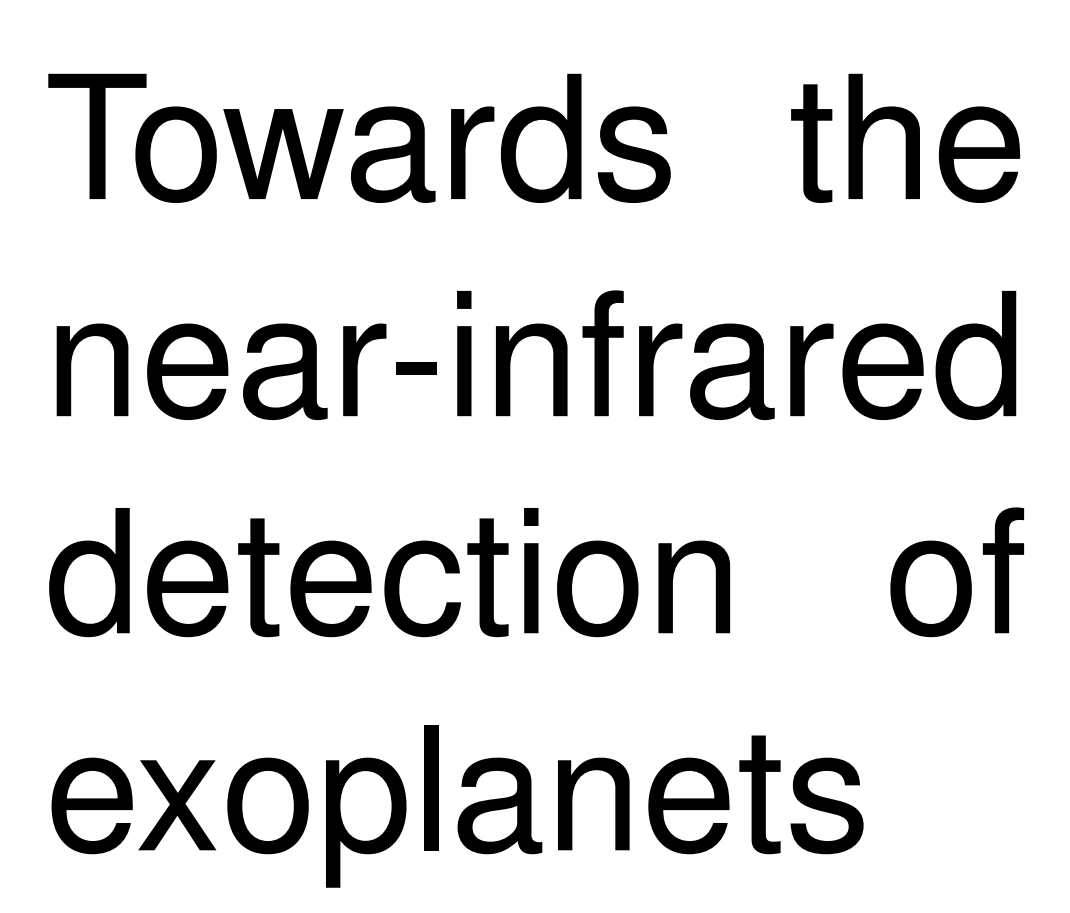
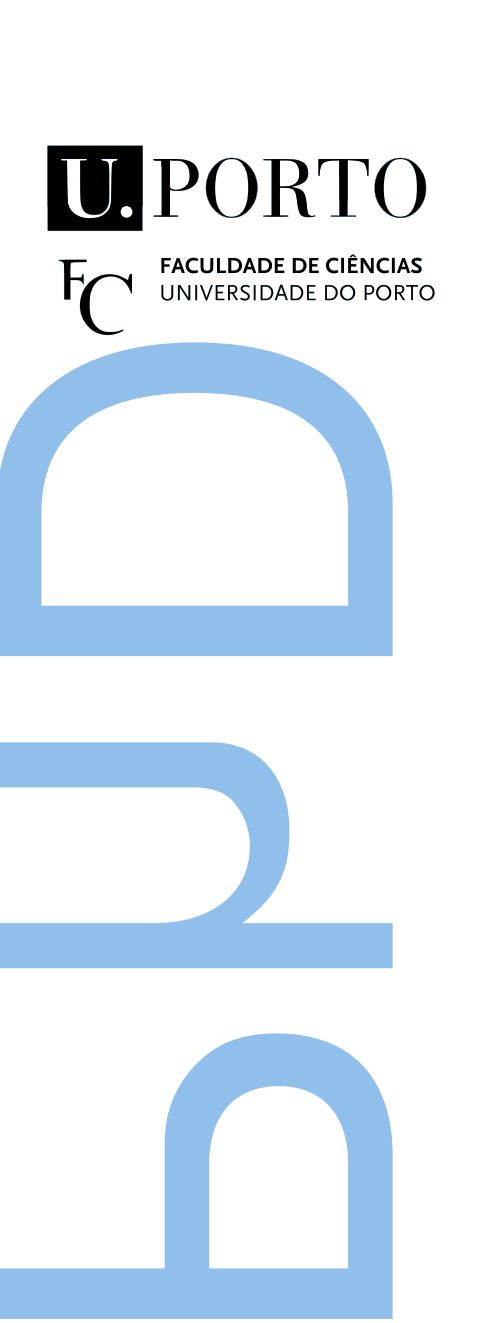
FCUP 2018



Jason James Neal

Tese de doutoramento apresentada à Faculdade de Ciências da Universidade do Porto Astronomia 2018

FC



TOWARDS THE NIR DETECTION OF EXOPLANETS

by

Jason James Neal

A thesis submitted in conformity with the requirements for the degree of Doctor of Philosophy Graduate Department of Departamento de Física e Astronomia University of Porto

© Copyright 2018 by Jason James Neal

To my wife Jessica, children Timothy and Amelia; For always supporting me.

Acknowledgements

this work could not have been competed without the Phd fellowship.

J.J.N. acknowledges support from FCT though the PhD::Space fellowship PD/BD/52700/2014.

This work was financed by FEDER - Fundo Europeu de Desenvolvimento Regional funds through the COMPETE 2020 - Programa Operacional Competitividade e Internacionalização (POCI), and by Portuguese funds through FCT - Fundação para a Ciência e a Tecnologia in the framework of the project POCI-01-0145-FEDER-028953 and POCI-01-0145-FEDER-032113."

This work was also supported by Fundação para a Ciência e a Tecnologia (FCT) (Portugal) research grants through national funds and from FEDER through COMPETE2020 by the following grants: UID/FIS/04434/2013 & POCI-01-0145-FEDER-007672, PTDC/FIS-AST/1526/2014 & POCI-01-0145-FEDER-016886, and PTDC/FIS-AST/7073/2014 & POCI-01-0145-FEDER-016880.

Abstract

The contents of this work focus on detecting exoplanets in the nIR.

It starts of with reduction of nir spectra from CRIRES.

In chapters 4 we approach a differential subtraction technique to separate the spectra from the faint companion. Contrasting the result to other recent detections. In chapter 4 a second technique is developed in which the BD companions are attempted to be recovered from the \nearrow -infrared spectra by fitting to a complex model of two synthetic stellar spectra. Finding the technique unsuitable for the data on hand.

Focusing on BD as they should have a stronger flux ratio than planets.

In chapter 6 we change focus towards RV precision of M-dwarf starts. Calculating the theoretical precision of stellar spectra t. Useful for the next-generation of near-infrared spectrographs to detect planets around M-dwarf stars.

Some thought on future are also provided.

Resumo

Thesis abstract in Portuguese

Todo list

	read and quote	4
Fi	gure: example to point to	5
	finish this	6
	Add original caption to 1.4	6
	Move location / adjust from paper	10
	this section is completed i think	12
	this section is completed i think	13
	ADAPT THis section to explain the models more generally. Move the usage back to Reduction	
	section	13
	telluric model correction methods original	13
	Look at	14
	FINISH	14
	FINISH	14
	a good reference that mentions the uv and optical uses could be good?	14
		16
	I don't know where I am going with this section	17
		17
	FIXup this table	18
	fix Figure 3.3	18
	move	18
	Check if it is mentioned how these get corrected/ if the impact the wavelength solution	19
	Note: Useful information about MIR reduction in the VISIR manual	19
	Reword	20
	Pedro it is my understanding that the ESO pipeline did not exist/was not publicly available	
	when you created DRACS, correct?	20
	is footnote correct "instruments optics"	22
	Check optimal extraction parameters, may have reduced the extraction width by too much??	
	Need to check changing it	24
	finish this sentence in caption	25
	CHANGE the figure here	26
	check this statement	26

	citation	27
	citation	27
Fi	gure: An image of some reduced spectra from eta Tel and Barnard's star????	27
	fix-up get a good citation, number of lines	28
	paper for harps Th-Ar lines	28
	cite crires manual, and a paper about sky lines?	28
Fi	gure: example figures illustrating this method	29
Fi	gure: Example of coordinates and the fit. Can I calculate some errors on the polynomial coord fit.	29
	explain the fit Figure 3.8	30
Fi	gure: Would a table of polynomial wavelength solutions along with errors be any use?	31
	Add pictures of wavelength calibrations	31
Fi	gure: Diagram of idea of combined detector fitting?	31
Fi	gure: comparison between a Gasgano wavelength solution and the manual one. This has not be	
	done by me before	32
	See Solene's paper regarding Telluric correction with models and reference spectra	32
	See solenes paper for matereial here	33
	Expand this section	33
	Should this be more in the introduction?	33
Fi	gure: The telluric spectrum around $2\mu\mathrm{m}$ showing the $2.1\mu\mathrm{m}$ window of low telluric absorption .	33
	Add telluric spectra for nIR band? the plot from Molecfit?	34
	Still uneven line coverage on all detectors in this small range	34
	$\mathrm{H_2O}$ corrections	34
	ADAPT this section to the usage of the models	34
	telluric model correction methods original	34
	ADD non-H $_2{\rm O}$ fitting corrections	36
Fi	gure: Plots showing some examples the telluric correction with and without ${\rm H_2O}$ separated	36
	Rotate orbital parameter table	38
	I still assume this is a mistake	39
	Check why the ordering number is incorrect for HD202206. If it is correct like this and is	
	numbered incorrectly in the header then we should mention this	39
	rotate table?	39
	I am not sure if this is the best location for this section	40
	equations for companion rv with the masses still included. include 180 degree angle phase	
	change also	40
	Fix caption position here	40
	recalculate values that are less than 1	40
	put in advanced concepts chapter???	42
	this ignores γ	42
Fi	gure: simulated example of combined binary spectra, and the subtraction, with a clear companion	
	visible	43
	Should I predict when the best time to observed these targets are is? e.g. in 2020 x and x will	
	have sufficient RV change in one period to achieve a detection	46
	change RV scale for hd4747 orbit	46

	Fix plot titles	46
	Check M2sini labels - can we get M2 only for those that we know	
	Should RV of companion be scale by m2sini only or m2 if known?	
	Increase size of diff amp plots to two	
	They get a result???	
	move	
Fig	gure: includegraphics images/HD211847 example pcolors.pdf	
-	gure: includegraphics images/HD211847 example pcolors.pdf	60
	gure: images HD211847 result pcolors.pdf	
-	gure: images/visualize result residuals.pdf	
	gure: images/inject recovery hd30501.pdf	
	gure: images/chi2 shape investigation sigmas.pdf	
	finish this line	
	Try cross correlation at a different wavelength 2.3 micron?	
	Try cross correlation with much larger wavelength range. 50, 100, 600, 1000 nanometres?	
	Try my simulations with much larger wavelength range. 50, 100, 600 nanometres?	69
	this doesn't seem right	70
	rv method	70
	put in introduction??	70
	Check mission statements for these	70
	For example from Figueira 2016 see figure	70
Fig	gure: An example from Figueira et al. 2016	
	find mayor queloz precision achieved	71
	what reference	71
	History of Precision calculations	71
	add δA to plots	72
	intensity change from connes is vertically in the slice d lambda	72
	Finish this equation (9 of bouchy 2001)	74
	Try the symbolic package from PC	74
	explain snr	75
	It is convenient to use this version when comparing observed spectra with different S/N.?	75
	Does spectrograph pipelines such as HARPS use these equations to measure estimate/precision?	75
	It is convenient to use this version when comparing observed spectra with different S/N.?	76
	top view diagram of rotation?	76
	define $fwhm0$	77
	CHECKTHISRESUSLT!!!!!!	77
Fig	gure: Example of CARMENES spectra before and after correction	78
	Add figure here	79
	Add figure here	79
	finish this	79
	works of software testing in research	82
Fig	gure: uncomment this one	84
	cite the equation when I refer to it	87

	Check this if it is previous	88
	weighted sum equation	88
	Should I show the working of analytical working out of this in an appendix, or here?	88
	did I check this was equivalent	88
	put this some where	88
	put this line elsewhere	88
	add conclusions not affected	89
	is this needed	90
	SNR plot/diagram	90
	Check how to cite priv communication properly	9
	Inlcude correct links	9
	comparison of plots	9
	NIR analysis work	94
	Precision table needs fixed up	95
	check direction and magnitude in table	96
	Maybe transpose Table B.1 to be shorter?	98
] CHANGE $\#$ into the ESO identification number 1b 2a etc	98
	Is this significant??	98
	is detector two significant as well?	98
	change scale on delta flux of HD 162020-2 chip 1 (it is too large atm)	98
Fi	gure: Corner plot of single detector?	104
Fi	gure: Corner plot fixed gaps	104
Fi	gure: Corner plot variable gaps	104
	remove vertical lines	104
	fill in table	105
Fi	gure: Residuals between individual fitting and the variable gap fits	105
	Fix up at end	106

Contents

To	Todo list vi								
Li	List of Tables xiii								
Li	st of	Figures	i						
1	Intr	roduction	1						
	1.1	Towards the characterization of Exoplanets	1						
	1.2	Detection methods	1						
		1.2.1 Radial Velocitmetry	2						
		1.2.2 Transit and TTV	3						
		1.2.3 Direct detection	3						
		1.2.4 Astrometry	3						
		1.2.5 Microlenseing	3						
		1.2.6 Detecting atmospheres	3						
		1.2.7 Transmission spectroscopy	3						
		1.2.8 Reflection in optical	3						
		1.2.9 Phase variations	3						
		1.2.10 High resolution spectroscopy	3						
		1.2.11 Stellar and planetary formation	3						
		1.2.12 Exoplanet distribution	3						
	1.3	Main Section 2	4						
	1.4	Recent detections in Companion spectra	1						
		1.4.1 model fitting transit stars (not actual title, more other similar methods)	1						
		1.4.2 Earths atmosphere	5						
	1.5	Paper Introduction	3						
	1.6	Motivation)						
2	Fun	ndamental concepts about spectroscopy and RV 10)						
		2.0.1 RV calculation)						
	2.1	Estimating Companion-host Flux ratio	1						
		2.1.0.1 Raraffo tables)						

		2.1.1	Companion K
	2.2	Telluri	c correction
		2.2.1	Telluric models
			2.2.1.1 TAPAS
		2.2.2	Tapas models
	2.3	Synthe	tic Stellar models
		2.3.1	PHOENIX-ACES
		2.3.2	BT-Settl
			2.3.2.1 Vacuum wavelengths
		2.3.3	Differential techniques
3			pic reduction 16
	3.1		ary of dataset
	3.2	_	ectroscopy
		3.2.1	General reduction Concepts
			3.2.1.1 Dark Current
			3.2.1.2 Flat-field
			3.2.1.3 Nodding and Jitter
		3.2.2	Th-Ar lamp calibration
		3.2.3	Extraction
	3.3	Pipelin	e Comparison
		3.3.1	ESO CRIRES pipeline
		3.3.2	DRACS
		3.3.3	Pipeline comparison and selection
			3.3.3.1 Reduction issues
		3.3.4	Reduction experience:
	3.4	Post re	duction stages
		3.4.1	Wavelength calibration
			3.4.1.1 Telluric correction
		3.4.2	Tapas models
		3.4.3	Issues with TAPAS
			3.4.3.1 Telluric masking
		3.4.4	Wavelength masking
		3.4.5	Barycentric correction
	C	, •	
4	_	_	the spectra of faint companions 37
	4.1		ues
	4.2		tion
	4.3		tion and target selection
		4.3.1	The Data
		4.3.2	CRIRES data
		4.3.3	Calculations using observed times
	4.4		Subtraction Method
		4 4 1	Results of spectral differential analysis

	4.5	Orbital S	olutions	44
		4.5.1 Re	elative differential amplitude	50
		4.	5.1.1 Differential scheduling challenges copy from paper	52
	4.6	Direct rec	covery in the mIR	52
	4.7	Summary		53
5	Con	npanion l	Recovery using synthetic models	54
	5.1	Main Sec	tion 1	54
	5.2	Binary sy	nthetic spectral recovery	54
		5.2.1 Sy	vnthetic PHOENIX-ACES models	54
		$5.2.2 \chi^2$	2 method	55
		5.2.3 Co	omputed model spectra	56
		5.	2.3.1 Single component model	56
		5.	2.3.2 Binary model	57
		5.	2.3.3 Effective radius	57
		5.2.4 Re	e-normalization	58
		5.2.5 Re	educing parameters	58
	5.3	Results.		60
		5.3.1 Si	mulated binaries	60
			D211847 observation	
			ompanion injection-recovery	
			unk from paper about BT-settl	
			cremental changes	
			ote about a target - discussion of results	
			3.6.1 Wavelength range	
6	Info	rmation	content of nIR Spectra	70
	6.1	Overview	·	70
	6.2	Radial ve	locity precision	7.
		6.2.1 Fu	undamental photon noise limitation	7.
		6.	2.1.1 summarize	76
		6.2.2 Pr	repare phoenix aces models	76
		6.2.3 Re	otation convolution	76
		6.2.4 In	strumental Convolution	77
		6.2.5 N	umerical Convolution	77
	6.3			78
		6.3.1 Ba	ands	79
		6.3.2 C	omparing models to CARMENES	79
	6.4	Metallicit	y NaN effects	80
	6.5		·	82
				82
				82
		6.5.3 M	odel extension	83
	6.6	Numerica	d Gradient	8:

	6.6.1 Masking Function	87
	6.6.1.1 Masking order	88
	6.6.2 Atmospheric masking bug	88
	6.6.3 SNR scaling	89
	6.7 SPIRou and NIRPS ETC	90
	6.8 Updated Figueira 2016 results	91
	6.9 metalicity / logg extension	91
	6.10 Application to CARMENES spectra	91
7	Conclusions	93
	7.1 Conclusions from Paper	93
	7.2 Future Work	94
\mathbf{A}	RV Precision Tables	96
В	Artefacts in Optimal Extraction	98
\mathbf{C}	Multi-dectector wavelength calibration	104
D	PhD output	106
	D.1 Publications	107
	D.2 Talks and Seminars	111
	D.3 Posters	112
	D.4 Attended Conferences and Schools	115
	D.5 Outreach	
	D.6 Other	
Bi	ibliography 1	119

List of Tables

2.1	Estimated flux ratios given the companion mass $(M_2 \text{ or } M_2 \sin i)$ from Table 4.2	12
4.1	Stellar parameters of the host stars. V is the apparent magnitude taken from SIM-BAD (Wenger et al., 2000). Distances were calculated from the GAIA DR2 parallax measurements	38
4.2	Orbital parameters for the BD companions obtained from the literature. Yes need rotating.	39
4.3	Details about the each CRIRES observation. The number of artefacts removed in Section 3.3.3.1 as well as the SNR of the combined spectra is provided. The last three columns are the calculated RV of both host and largest companion, from the orbital solution, as well as the RV difference between the two components	40
4.4	Estimated orbital semi-amplitude and RV separation of the companion, given the companion mass $(M_2 \text{ or } M_2 \sin i)$ from Table 4.2 and observation times from Table 4.3	41
5.1	Full parameter space of the PHOENIX-ACES spectral grid	55
5.2	Input and recovered parameters on simulations and an observation when applying a single (C ¹) and binary (C ²) models. The logg and metallicity were fixed at $logg_1 = 4.50$, $logg_2 = 5.0$ and [Fe/H]=0.0 equally for both components. Gaussian noise was added to both simulations with a SNR of 150. Here m and n are the number of data points and parameters used in each model	59
5.3	Upper mass limits of target companions assuming a companion logg=5.0. Masses are derived from Baraffe et al. (2015) evolutionary models using $T_{\rm eff}$ and logg. The flux ratio F_2/F_1 is the absolute flux ratio between the cut-off temperature and the target host star.	66
6.1	The wavelength ranges of the nIR spectral bands	79
6.2	CARMENES library target selection spanning the M-dwarf spectral range	79
6.3	csv2tex table	80

6.4	The affect of the numerical gradient function on RV precision. The band label VIS and NIR indicate the full visible and nIR bands while $CARM_{VIS}$ and $CARM_{NIR}$ indicate the two wavelength bands of the CARMENES spectrograph. $\Delta\lambda$ is a wavelength shift applied to move the FFD values between pixels for this comparison only. The M0 spectra used here had no rotation, or instrument broadening preformed and was normalized to a maximum of 1 in each band. The precision values given here are for accessing the relative precision	
6.5	change due to the different gradient methods	
A.1	RV precisions from the PHOENIX-ACES and BT-Settl synthetic spectral libraries. The PHOENIX-ACES values are the updated values from Table A.1 of Figueira et al. (2016).	0.6
A.1	continued	
A.1		
A.1	continued.	
A.1	continued.	
A.2	continued	
A.2	continued.	
A.2	continued.	
A.2		
A.2	continued	
A.2		
A.2	continued	
A.2	continued.	
A.2	continued	. 11:
A.2	continued	. 112
A.2	continued	. 113
A.2	continued	. 114
A.3	RV precisions calculated for the SPIRou ETC. Same simulations as Table A.1 but with	
	the SNR relative to the centre of each individual band	. 114
A.3	continued	. 115
A.3	continued	. 116
A.3	continued	. 117
A.3	continued	. 118
A.3	continued	. 119
B.1	Identification of all the optimally reduced nod spectra which had artefacts that were replaced by the rectangular extractions, corrected for bad pixels. The numbers represent the position in the nod cycle ABBAABBA. The number of the observation for each target is given by $\#$	90

В.2	Tally of nod cycle positions in which their optimally reduced spectra were affected and	
	were replaced	99
C 1	Example fitting parameters obtained for HD30501 observation 2 under different scenarios 10	05

List of Figures

1.1	Number of exoplanet detections per year separated by method (data from exoplanet.eu October 2018)	2
1.2	Distance mass diagram (data from exoplanet.eu October 2018)	4
1.3	M-R relationship Chen and Kipping (2016)	5
1.4	Reproduction of Figure 1 of Smette et al. (2015) showing telluric absorption form 0.30 µm. Original caption:	7
2.1	By Lasunncty at the English Wikipedia, CC BY-SA 3.0, https://commons.wikimedia.org/w/index.pdf	dex.php?curid=8971
3.1	Master dark frames for exposure times of 3 and 180 seconds. Each master is created by averaging 3 images in which the detector received no incident light. Both frames are on the same scale and show dark current grows with exposure time. The colour has been inverted so that black is the recorded measurement	17
3.2	A flat-field image for detector #2 before (left) and after (right) the non-linearity corrections are performed	18
3.3	Illustration of the nodding technique. Left: Sample slice of successive images at nod positions A and B, and their difference A-B for detector #1. Right: A vertical slice along the slit at column 512 (middle of detector). The background level observed in A and B is	
	effectively removed by the subtraction	19
3.4	Example Th-Ar calibration lamp frames for each detector. These are the raw frames in which dark current correction has not been performed (i.e the dark current is still visible	
	,	20
3.5	Comparison between the ESO pipeline and DRACS pipeline. For two observations HD30501-1 and HD202206-1. The blue lines are the extracted spectra from the ESO pipeline, the orange dashed lines are the optimal extraction from the DRACS pipeline, while the green dash-dotted line is the DRACS extraction after dealing with artefacts in the optimal extraction addressed in Section 3.3.3.1. The wavelength information applied	22
	to the spectra here comes from the ESO pipeline	23

3.6	Left: Pipeline with the "doslit.resize" set to "no". Right: The same but with "doslit.resize" set to "yes". During the order tracing the aperture size is automatically adjusted but the finish this sentence. Setting the resize parameter for apextract?. Changing this one parameter removed one large artefact but kept the other. One large artefact is removed, one is not	25
3.7	Example of an artefact in the optimally extracted spectra from detector #2 of HDXXXXXX. The top panel contains the 8 normalized nod spectra obtained using optimal extraction. The middle panel shows nod spectra using only rectangular extraction. The bottom panel shows the difference between a combined spectrum using optimal nods only and a combined spectrum in which the identified nods are replaced with their rectangular counterparts as per Section 3.3.3.1. A vertical offset is included between each spectra for clarity. The nod spectra are in observation order from top to bottom	26
3.8	Wavelength calibration example. The equation of the fitted line for these points is $\lambda = -1.85e^{-7}x^2 + 1.16e^{-2}x + 2111.86 \text{ with each coefficient shown to two decimal places}$ only. Error bars the line width set to around 0.04 nm	30
3.9	An example spectra for each target and each detector 1–4 in order of increasing wavelength. The solid lines are the spectra while the black dashed lines are the telluric models used for	96
	wavelength correction, showing good alignment with the spectra	32
4.1	(Top) A reduced CRIRES observation of HD 30501 (blue) for detector 1 between 2112–2124 nm along with the tapas telluric absorption model (orange dashed) used for the wavelength calibration and telluric correction. (Middle) The telluric corrected spectra. (Bottom) (blue) Differential spectra for HD 30501 between observations 1 and 3. (orange dashed) Simulated "perfect" differential using PHOENIX-ACES spectra with parameters $T_{\rm eff}=2500{\rm K},\log = 5.0, {\rm and} [{\rm Fe/H}] = 0.0, {\rm with}{\rm the}{\rm same}\Delta RV$ as the observations. The shaded regions indicate where the telluric green and host star blue spectra are $>4\%$ deep.	45
4.2	RV orbital single companion Keplerian for the HD 4747. The left hand plot shows the RV curve for one full orbit while the right hand panel shows the RV curve over 6 months (Period 89). The solid black line indicates the RV of the host star (with scale on the left), while the blue dashed line indicates the RV of the companion (with scale on the right axis). The orange crosses and red stars indicate the times at which observations were obtained for the target, for the host and companion respectively.	45
4.3	Same as Figure 4.2 but for HD 162020	
4.4	Same as Figure 4.2 but for HD 167665	
4.5	Same as Figure 4.2 but for HD 168443b. Analysed as if this was a single companion	
4.6	Same as Figure 4.2 but for HD 168443c. Analysed as if this was a single companion	48
4.7	Same as Figure 4.2 but for HD 202206B. Analysed as if this was a single companion	48
4.8	Same as Figure 4.2 but for HD 202206c. Analysed as if this was a single companion	49
4.9	Same as Figure 4.2 but for HD 211847	49
4.10	Same as Figure 4.2 but for HD 30501	49

4.11	Simulated relative amplitude of differential spectra at different companion ΔRV separations revealing the diminished amplitude at very small orbital separations. The solid blue line shows the maximum relative amplitude of the differential signal (from a shifted copy of itself) of a PHOENIX-ACES spectrum with $T_{\rm eff}=2500\rm K$, logg=5.0, [Fe/H]=0.0 in the wavelength region 2110–2123 nm. The maximum difference is normalized by the median amplitude between ± 7 –10 km s ⁻¹ , representing a complete line separation. The orange (dashed) and green (dot-dashed) lines represent the relative amplitude of a differential spectrum of a spectrum containing a single Gaussian and single Lorentzian absorption line respectively, each with a unitary amplitude and a FWHM = λ/R . The solid vertical lines indicate the estimated companion ΔRV in these observations while the dashed vertical lines indicate the RV corresponding to the FWHM at this wavelength and resolution	51
5.1	χ^2 results for companion recovery of a simulated binary observation of a Sun-like star $(T_{\rm eff1}=5800{\rm K})$ with an M-dwarf companion $(T_{\rm eff2}=4000{\rm K})$. The top right plot shows the application of a single component model (C^1) while the other three are using a binary model (C^2) . Both left hand panels show the distribution of host temperature and host RV. The top right panel shows the distribution for host and companion temperature, and the bottom right the companion temperature and radial velocity. The red circle and yellow star indicate the location of the simulation input and recovered parameters respectively. The white line shows a 3- σ confidence level about the minimum χ^2 solution grid point. Each box is centred on the parameter values and shows the grid resolution	60
5.2	Similar to Figure 5.1, χ^2 results for companion recovery of a simulated binary observation similar to HD 211847, $(T_{\rm eff_1}=5800{\rm K},T_{\rm eff_2}=3200{\rm K})$. The top right plot shows the application of a single component model (C^1) while the other three are using a binary model (C^2) . Both left hand panels show the distribution of host temperature and host RV. The top right panel shows the distribution for host and companion temperature, and the bottom right the companion temperature and radial velocity. The red circle and yellow star indicate the location of the simulation input and recovered parameters respectively. The white line shows a 3- σ confidence level about the minimum χ^2 solution grid point. Each box is centred on the parameter values and shows the grid resolution	60
5.3	χ^2 result grid for observation 2 of HD 211847, similar to Figs. 5.1 and 5.2. The top right plot shows the application of a single component model (C^1) while the other three are using a binary model (C^2) . Both left hand panels show the distribution of host temperature and host RV. The top right panel shows the distribution for host and companion temperature, and the bottom right the companion temperature and radial velocity. The red circles indicate the literature values or calculated parameters for the target while the yellow star indicates the minimum χ^2 solution. The error bar on the $T_{\rm eff1}$ is from the literature while the error bars on rv_1 and rv_2 are calculated by propagating the orbital parameter uncertainties though the radial velocity equation. The white line shows a 3- σ confidence level about the minimum χ^2 solution grid point, not always visible here due to the large χ^2 values	63

5.4	Comparison between the observed HD 211847 spectrum (blue) and the best fit synthetic binary model (orange dashed) for each detector. The bottom section of each panel shows the residuals between the parts of the observation used in the χ^2 fit and recovered binary model (O – C ²) in purple. The red dashed line shows the difference between the recovered binary model and the binary model with the exact same parameters except for the estimated companion temperature of $3200\mathrm{K}$ (C ² [$3200\mathrm{K}$] – C ²). The grey shading indicated the wavelength regions where masking has been applied. The thinner masked regions that match with cuts in the observed spectra are where the centres of deep (>5%) telluric lines that have been masked out are	64
5.5	Result of simulated injection-recovery of synthetic companions on HD 30501. The blue dots and orange triangles indicate the recovered companion temperature for the observed and synthetic spectra respectively. The $\pm 100\mathrm{K}$ error bars are the grid step of the synthetic models. The black dashed diagonal shows the 1:1 temperature relation. The grey shaded region indicates the $\pm 1000\mathrm{K}$ temperature range explored. Gaussian noise added to the synthetic spectra was derived from the observed spectra	65
5.6	(top) Companion temperature verses χ^2 for simulations with different injected companion temperatures. Other fixed parameters for these fully synthetic simulations was $T_{\rm eff1}=5200{\rm K},\log\!g_1=4.5,\log\!g_2=5.0,$ and both [Fe/H]=0.0. A fixed Gaussian noise corresponding to a SNR of 300 was used. (bottom) A close up view of $\chi^2<15$. The three horizontal grey lines indicate the 1, 2, 3 sigma with 2 degrees of freedom. The vertical dotted lines indicate the location of the minimum χ^2 recovered for each companion. The black solid vertical in both panels shows the 2 300 K cut-off of the PHOENIX-ACES models	65
6.1	Mass of discovered planets verse year. From Exoplanet.eu	72
6.2	Arbitrary spectral line with a shift $\delta\lambda$, inspired by Connes (1985). Λ is the wavelength range considered	73
6.3	Quality factor changes across spectral type and bands for variations in [Fe/H] and NaN. Broadening values are R=100 000 and $v \sin i = 1.0 \mathrm{kms^{-1}}$. Top: Quality factor variation of [Fe/H] between -1.0 to 1.0 at a fixed NaN=4.5. Bottom: Quality factor variation of NaN between 4 and 5.5 with fixed [Fe/H]=0.0. Note a higher quality factor corresponds to an increased RV precision	81
6.4	Visualization of the numerical gradient of some spectral lines. Top: The two spectral regions of a stellar spectrum the left hand slide contains short lines near the normalized continuum while on the right a single deep absorption line is shown. Bottom: The numerical gradients for the spectra shown in the top panels; the original FFD method is displayed with <i>blue squares</i> while numpy gradient is shown with <i>green stars</i> . The <i>orange circles</i> are the FFD version shifted to the mid-points between pixels for illustrative purposes	85
6.5	Left: Figueria et al 2016, Right, Updated values from this work computed with eniric	9:

B.1	Artefact example for the second detector of HD 4747. The top panel contains the eight	
	normalized nod spectra obtained using optimal extraction. The middle panel shows nod	
	spectra using only rectangular extraction. The bottom panel shows the difference between	
	a combined spectrum using optimal nods only and a combined spectrum in which the	
	identified nods are replaced with their rectangular counterparts as per Section 3.3.3.1.	
	A vertical offset is included between each spectra for clarity. The nod spectra are in	
	observation order from top to bottom. In this example there are artefacts in the 5th	
	(purple) and eighth (grey) nod spectra around 700 and 500 pixels respectively	100
B.2	Same as Figure B.1 but for the first detector of the second observation of HD 162020. In	
	this example there are several large spikes observed in the rectangular extraction but they	
	do not appear to effect the optimally extracted nods. reduce scale of delta flux (to large	
	<u>atm</u>)	101
В.3	Same as Figure B.1 but for the third detector of the second observation of HD 167665. In	
	this example a small spike in the first spectrum (blue) around pixel 450 causes a extended	
	dip in the optimally extracted nod	101
B.4	Same as Figure B.1 but for the 1st detector of the second observation of HD 202206. In	
	this example there are several large spike but only one produces an artefact. This is on	
	the 5th nod (purple) around pixel 800	102
B.5	Same as Figure B.1 but for the fourth detector of the first observation of HD 168443. In	
	this example a barely visible spike on the 7th nod (pink) causes a deviation in the optimal	
	nod around pixel 610. There is also a second small spike on the eighth nod (grey) around	
	pixel 850, between two spectral lines	102
B.6	Same as Figure B.1 but for the second detector of the second observation of HD 211847.	
	In this example two large spikes around 800 and 1000 in the 7th nod (pink) create large	
	deviations in the optimally reduced spectra. A spike in the first nod (blue) around pixel	
	700 also causes a bump. There is also some extra noise in the first nod around pixel 350 .	103
B.7	Same as Figure B.1 but for the second detector of the second observation of HD 30501.	
	In this example there are artefact causing spikes in four places. The second nod (orange)	
	around pixel 950, the 6th nod (brown) around pixel 20 and two spikes in the 7th nod	
	(pink) around pixels 400 and 550	103

Precision table needs fixed up



RV Precision Tables

The updated relative RV precision results attainable from nIR spectra are presented in the following tables. Table A.1 shows the precision results for the same M-dwarfs analysed in (Figueira et al., 2016). That is stellar temperatures 3900, 3500, 2800, 2600K corresponding to spectral types M0, M3, M6, M9 respectively. $\log = 4.5$ and [Fe/H] = 0.0. The rotation applied are $v \sin i = 1$, 5, $10 \, \mathrm{km \, s^{-1}}$ and instrumental profiles with $R = 60 \, \mathrm{k}$, 80k, 100k.

Columns 2-4 contain the RV precision calculated using PHOENIX-ACES spectra, as done in Figueira et al. (2016). These values differ from two effects. There is small difference in Conditions 1 and 3 from the change in numerical differentiation implemented (see Section 6.6). The values for Condition 2 however, are completely different due to the implementation error in the telluric masking discovered (see Section ??).

In columns 5-7 are the same RV precision calculation but using the BT-Settl spectral library instead (with same spectral parameters), a recent addition in *eniric*.

These can be created with *eniric* with the following shell incantation (after installation and configuration).

```
phoenix_precision.py -t 3900 3500 2800 2600 \ # Temperature
-1 4.5 -m 0.5 \ # Logg and Metalicity
-r 60000 80000 100000 \ # Resolutions
-v 1.0 5.0 10.0 \ # Rotational velocities
-b Z Y J H K \ # Wavelength bands
--snr 100 \ # Relative SNR
--ref_band J # SNR reference band
```

eniric was also used to calculate RV precision for the NIRPS and SPIRou.

For SPIRou the requested precisions were provided with the SNR relative to the centre of each individual band. The values are provided in Table A.3 and can be generated with the following code, note the change in.

This has the effect of Z Y band precisions being **lower** and H and K band precisions being **higher**. compared to Table ??

```
check direction
and magnitude
in table
```

```
phoenix_precision.py -t 3900 3500 2800 2600 -l 4.5, \rightarrowm 0.5 \ -r 60000 80000 100000 -v 1.0 5.0 10.0 -b Z Y J H K
```

```
--snr 100 --ref_band self
```

For NIRPS RV precisions with an instrumental resolution of $75\,000$ was requested to match the NIRPS instrument, and provided relative to the J and H-bands. The results for the NIRPS precision relative to the J-band are given in Table $\ref{Table 1}$, and can be reproduced with the following code.

```
phoenix_precision.py -t 3900 3500 2800 2600 -l 4.5, -m 0.5 \
-r 60000 75000 80000 100000 -v 1.0 5.0 10.0 \
-b Z Y J H K --snr 100 --ref_band H
```

Table A.1: RV precisions from the PHOENIX-ACES and BT-Settl synthetic spectral libraries. The PHOENIX-ACES values are the updated values from Table A.1 of Figueira et al. (2016).

	PHOENIX-ACES			BT-SETTL		
Simulation	Cond. 1	Cond. 2	Cond. 3	Cond. 1	Cond. 2	Cond. 3
(SpTp - Band - v.sini - R)	$\sigma_{RV}[{ m m/s}]$	$\sigma_{RV} [\mathrm{m/s}]$	$\sigma_{RV} [\mathrm{m/s}]$	$\sigma_{RV} [\mathrm{m/s}]$	$\sigma_{RV}[{ m m/s}]$	$\sigma_{RV} [\mathrm{m/s}]$
3900-Z-1.0-60k	9.7	15.5	10.0	9.4	15.3	9.7
3900-Z-1.0-80k	6.4	10.4	6.6	6.6	10.7	6.8
3900-Z-1.0-100k	4.7	7.8	4.9	5.2	8.5	5.3
$3900\text{-}Z\text{-}5.0\text{-}60\mathrm{k}$	14.2	22.6	14.6	13.0	21.0	13.4
$3900\text{-}Z\text{-}5.0\text{-}80\mathrm{k}$	10.9	17.6	11.3	10.1	16.4	10.5
$3900\text{-}Z\text{-}5.0\text{-}100\mathrm{k}$	9.2	14.8	9.5	8.6	13.9	8.9
$3900\text{-}Z\text{-}10.0\text{-}60\mathrm{k}$	24.5	38.6	25.3	21.8	35.1	22.4
$3900\text{-}Z\text{-}10.0\text{-}80\mathrm{k}$	20.3	32.2	21.0	18.1	29.2	18.7
3900-Z-10.0-100k	17.8	28.2	18.3	15.9	25.6	16.3
3900-Y-1.0-60k	9.6	11.5	9.8	12.5	15.0	12.7
3900-Y-1.0-80k	6.0	7.1	6.0	8.3	10.0	8.4
3900-Y-1.0-100k	4.2	5.1	4.3	6.3	7.5	6.3
3900-Y-5.0-60k	15.5	18.4	15.7	18.6	22.3	18.9
3900-Y-5.0-80k	11.6	13.8	11.8	14.3	17.0	14.4
3900-Y-5.0-100k	9.7	11.5	9.8	11.9	14.3	12.1
3900-Y-10.0-60k	30.8	36.8	31.2	34.8	41.6	35.2
3900-Y-10.0-80k	25.2	30.1	25.5	28.6	34.3	29.0
3900-Y-10.0-100k	21.8	26.0	22.1	24.9	29.9	25.2
3900-J-1.0-60k	15.7	41.7	16.6	16.2	45.6	17.1
3900-J-1.0-80k	10.5	26.9	11.0	11.5	31.4	12.2
3900-J-1.0-100k	7.9	19.6	8.3	9.2	24.4	9.7
3900-J-5.0-60k	22.7	63.6	24.0	21.8	65.6	23.1
3900-J-5.0-80k	17.5	48.1	18.5	17.1	50.2	18.2
3900-J-5.0-100k	14.8	40.3	15.6	14.6	42.1	15.4
3900-J-10.0-60k	38.6	122.9	41.0	35.4	122.3	37.7
3900-J-10.0-80k	32.0	100.7	34.0	29.5	100.5	31.4
3900-J-10.0-100k	28.0	87.6	29.8	25.9	87.5	27.6
3900-H-1.0-60k	7.2	11.4	7.4	7.6	11.9	7.8
3900-H-1.0-80k	5.0	8.0	5.1	5.4	8.4	5.5

Table A.1: continued.

	PHOENIX-ACES			BT-SETTL		
Simulation	Cond. 1	Cond. 2	Cond. 3	Cond. 1	Cond. 2	Cond. 3
3900-H-1.0-100k	4.0	6.3	4.0	4.2	6.6	4.3
3900-H-5.0-60k	10.1	15.9	10.3	10.8	16.8	11.0
3900-H-5.0-80k	7.9	12.4	8.0	8.3	13.1	8.5
3900-H-5.0-100k	6.6	10.5	6.8	7.0	11.0	7.2
3900-H-10.0-60k	17.5	27.3	17.9	18.8	29.4	19.2
3900-H-10.0-80k	14.5	22.7	14.9	15.6	24.4	16.0
3900-H-10.0-100k	12.7	19.9	13.0	13.6	21.3	14.0
3900-K-1.0-60k	14.5	63.7	15.5	13.7	63.2	14.6
3900-K-1.0-80k	9.7	43.6	10.4	9.6	45.2	10.3
$3900\text{-}\mathrm{K}\text{-}1.0\text{-}100\mathrm{k}$	7.4	33.6	8.0	7.6	36.1	8.1
$3900\text{-}\mathrm{K}\text{-}5.0\text{-}60\mathrm{k}$	21.7	90.3	23.2	19.4	85.4	20.8
$3900\text{-}\mathrm{K}\text{-}5.0\text{-}80\mathrm{k}$	16.6	70.0	17.7	15.0	67.0	16.1
$3900\text{-}\mathrm{K}\text{-}5.0\text{-}100\mathrm{k}$	13.9	59.2	14.8	12.6	56.9	13.5
$3900\text{-}\mathrm{K}\text{-}10.0\text{-}60\mathrm{k}$	39.4	155.8	42.1	34.2	142.8	36.6
$3900\text{-}\mathrm{K}\text{-}10.0\text{-}80\mathrm{k}$	32.6	128.9	34.9	28.4	118.5	30.4
3900-K-10.0-100k	28.5	112.5	30.5	24.8	104.0	26.6
$3500\text{-}Z\text{-}1.0\text{-}60\mathrm{k}$	8.4	13.9	8.7	8.4	14.0	8.6
$3500\text{-}Z\text{-}1.0\text{-}80\mathrm{k}$	5.2	8.8	5.4	5.6	9.4	5.7
$3500\text{-}Z\text{-}1.0\text{-}100\mathrm{k}$	3.7	6.3	3.8	4.2	7.1	4.3
$3500\text{-}Z\text{-}5.0\text{-}60\mathrm{k}$	13.2	21.3	13.6	12.3	20.1	12.7
$3500\text{-}Z\text{-}5.0\text{-}80\mathrm{k}$	10.0	16.4	10.3	9.4	15.5	9.7
$3500\text{-}Z\text{-}5.0\text{-}100\mathrm{k}$	8.3	13.6	8.6	7.9	13.0	8.2
$3500\text{-}Z\text{-}10.0\text{-}60\mathrm{k}$	24.6	39.1	25.4	21.9	35.1	22.5
$3500\text{-}Z\text{-}10.0\text{-}80\mathrm{k}$	20.3	32.4	20.9	18.1	29.1	18.6
$3500\text{-}Z\text{-}10.0\text{-}100\mathrm{k}$	17.6	28.2	18.2	15.8	25.4	16.3
3500-Y-1.0-60k	8.5	10.1	8.6	11.3	13.3	11.4
3500-Y-1.0-80k	5.2	6.2	5.2	7.4	8.7	7.4
3500-Y-1.0-100k	3.6	4.3	3.7	5.5	6.5	5.5
3500-Y-5.0-60k	13.9	16.5	14.1	17.1	20.2	17.3
3500-Y-5.0-80k	10.4	12.3	10.5	13.0	15.3	13.1
3500-Y-5.0-100k	8.6	10.2	8.7	10.9	12.8	11.0
3500-Y-10.0-60k	28.2	33.5	28.5	32.4	38.4	32.8
3500-Y-10.0-80k	23.0	27.3	23.3	26.7	31.5	27.0
3500-Y-10.0-100k	19.9	23.6	20.1	23.2	27.4	23.5
3500-J-1.0-60k	15.1	38.4	15.9	16.7	47.9	17.8
3500-J-1.0-80k	9.8	24.0	10.3	11.8	32.6	12.5
3500-J-1.0-100k	7.1	17.1	7.5	9.3	25.1	9.9
3500-J-5.0-60k	22.5	60.2	23.8	22.9	69.2	24.4
3500-J-5.0-80k	17.3	45.4	18.3	17.9	52.9	19.0

Table A.1: continued.

	PHOENIX-ACES			BT-SETTL		
Simulation	Cond. 1	Cond. 2	Cond. 3	Cond. 1	Cond. 2	Cond. 3
3500-J-5.0-100k	14.5	37.8	15.3	15.2	44.4	16.2
3500-J-10.0-60k	39.9	117.8	42.4	37.9	129.4	40.5
3500-J-10.0-80k	33.0	96.4	35.1	31.5	106.4	33.7
3500-J-10.0-100k	28.8	83.7	30.6	27.6	92.6	29.5
3500-H-1.0-60k	7.7	12.4	7.9	7.7	12.4	7.9
3500-H-1.0-80k	5.4	8.8	5.6	5.4	8.8	5.5
3500-H-1.0-100k	4.3	6.9	4.4	4.3	6.9	4.4
$3500 ext{-H-}5.0 ext{-}60 ext{k}$	10.7	17.1	10.9	10.9	17.5	11.2
3500-H-5.0-80k	8.3	13.3	8.5	8.4	13.5	8.6
$3500 ext{-H-}5.0 ext{-}100 ext{k}$	7.1	11.3	7.2	7.1	11.4	7.3
3500-H-10.0-60k	18.1	28.7	18.5	19.5	31.4	20.0
$3500\text{-H}\text{-}10.0\text{-}80\mathrm{k}$	15.0	23.9	15.4	16.1	26.0	16.6
$3500\text{-H-}10.0\text{-}100\mathrm{k}$	13.1	20.9	13.5	14.1	22.7	14.5
$3500\text{-} ext{K-}1.0\text{-}60 ext{k}$	13.5	49.0	14.4	12.1	43.8	13.0
$3500\text{-}\mathrm{K}\text{-}1.0\text{-}80\mathrm{k}$	9.0	32.7	9.6	8.4	30.1	8.9
$3500\text{-}\mathrm{K}\text{-}1.0\text{-}100\mathrm{k}$	6.8	24.8	7.3	6.5	23.3	7.0
$3500\text{-} ext{K-}5.0\text{-}60 ext{k}$	20.4	71.7	21.7	17.6	62.6	18.8
$3500\text{-}\mathrm{K}\text{-}5.0\text{-}80\mathrm{k}$	15.5	55.2	16.5	13.5	48.4	14.4
$3500\text{-}\mathrm{K}\text{-}5.0\text{-}100\mathrm{k}$	13.0	46.4	13.9	11.4	40.8	12.1
$3500\text{-}\mathrm{K}\text{-}10.0\text{-}60\mathrm{k}$	37.5	126.6	39.9	31.8	109.6	34.0
$3500\text{-}\mathrm{K}\text{-}10.0\text{-}80\mathrm{k}$	30.9	104.6	33.0	26.3	90.7	28.1
$3500\text{-}\mathrm{K}\text{-}10.0\text{-}100\mathrm{k}$	27.0	91.3	28.8	23.0	79.3	24.6
2800-Z-1.0-60k	4.4	8.4	4.5	4.0	7.6	4.2
2800-Z-1.0-80k	2.6	5.1	2.7	2.6	4.8	2.7
2800-Z-1.0-100k	1.8	3.6	1.9	1.9	3.5	1.9
$2800\text{-}Z\text{-}5.0\text{-}60\mathrm{k}$	7.2	13.7	7.5	6.3	11.7	6.6
2800-Z-5.0-80k	5.4	10.3	5.6	4.8	8.8	4.9
2800-Z-5.0-100k	4.4	8.5	4.6	4.0	7.3	4.1
$2800\text{-}Z\text{-}10.0\text{-}60\mathrm{k}$	14.6	27.3	15.2	12.6	22.8	13.0
2800-Z-10.0-80k	11.9	22.4	12.4	10.3	18.6	10.6
2800-Z-10.0-100k	10.3	19.3	10.7	8.9	16.2	9.2
2800-Y-1.0-60k	5.8	7.4	5.9	11.7	14.0	11.9
2800-Y-1.0-80k	3.7	4.8	3.8	7.6	9.1	7.7
2800-Y-1.0-100k	2.7	3.5	2.7	5.6	6.7	5.7
2800-Y-5.0-60k	8.7	10.7	8.8	17.7	21.3	17.9
2800-Y-5.0-80k	6.7	8.3	6.8	13.5	16.2	13.7
2800-Y-5.0-100k	5.6	7.0	5.7	11.3	13.6	11.4
2800-Y-10.0-60k	14.7	17.5	14.9	32.5	39.0	32.9
2800-Y-10.0-80k	12.2	14.6	12.4	26.8	32.1	27.1

Table A.1: continued.

-	PHOENIX-ACES			BT-SETTL		
Simulation	Cond. 1	Cond. 2	Cond. 3	Cond. 1	Cond. 2	Cond. 3
2800-Y-10.0-100k	10.7	12.8	10.8	23.3	28.0	23.6
2800-J-1.0-60k	8.8	23.2	9.3	11.0	31.7	11.8
2800-J-1.0-80k	5.5	14.4	5.8	7.6	21.5	8.1
2800-J-1.0-100k	4.0	10.2	4.2	5.8	16.3	6.2
$2800\text{-J-}5.0\text{-}60\mathrm{k}$	13.5	35.9	14.3	15.6	45.3	16.7
2800-J-5.0-80k	10.3	27.3	10.9	12.1	35.1	13.0
2800-J-5.0-100k	8.6	22.8	9.1	10.2	29.6	10.9
2800-J-10.0-60k	24.3	63.8	25.7	26.7	78.5	28.5
2800-J-10.0-80k	20.1	52.9	21.2	22.2	65.1	23.7
2800-J-10.0-100k	17.5	46.1	18.5	19.4	57.0	20.7
2800-H-1.0-60k	6.6	12.8	6.9	5.7	11.1	5.9
2800-H-1.0-80k	4.4	8.5	4.6	3.9	7.5	4.0
2800-H-1.0-100k	3.3	6.4	3.5	3.0	5.8	3.1
$2800 ext{-H-}5.0 ext{-}60 ext{k}$	9.8	18.8	10.2	8.4	16.4	8.7
$2800 ext{-H-}5.0 ext{-}80 ext{k}$	7.5	14.4	7.8	6.5	12.6	6.7
$2800 ext{-H-}5.0 ext{-}100 ext{k}$	6.3	12.1	6.5	5.4	10.5	5.6
2800-H-10.0-60k	17.8	34.7	18.4	15.6	31.0	16.2
2800-H-10.0-80k	14.7	28.7	15.2	12.9	25.5	13.3
2800-H-10.0-100k	12.8	25.0	13.3	11.2	22.2	11.6
$2800\text{-}\mathrm{K}\text{-}1.0\text{-}60\mathrm{k}$	8.2	27.0	8.7	7.1	22.9	7.5
$2800\text{-}\mathrm{K}\text{-}1.0\text{-}80\mathrm{k}$	5.4	17.9	5.7	4.8	15.6	5.1
2800-K-1.0-100k	4.0	13.5	4.3	3.7	12.0	4.0
$2800 ext{-}5.0 ext{-}60 ext{k}$	12.4	39.7	13.2	10.3	33.3	11.0
$2800 ext{-} ext{K-}5.0 ext{-}80 ext{k}$	9.4	30.5	10.0	7.9	25.6	8.4
$2800\text{-}\mathrm{K}\text{-}5.0\text{-}100\mathrm{k}$	7.9	25.6	8.4	6.6	21.5	7.1
$2800 ext{-}10.0 ext{-}60 ext{k}$	23.0	70.7	24.6	19.1	59.6	20.4
$2800 ext{-}10.0 ext{-}80 ext{k}$	19.0	58.5	20.3	15.8	49.3	16.8
$2800 ext{-} ext{K-}10.0 ext{-}100 ext{k}$	16.6	51.1	17.7	13.8	43.0	14.7
$2600\text{-}Z\text{-}1.0\text{-}60\mathrm{k}$	3.7	7.7	3.9	3.4	6.5	3.6
2600-Z-1.0-80k	2.2	4.6	2.3	2.2	4.2	2.3
$2600\text{-}Z\text{-}1.0\text{-}100\mathrm{k}$	1.5	3.2	1.6	1.6	3.0	1.7
$2600\text{-}Z\text{-}5.0\text{-}60\mathrm{k}$	6.1	12.5	6.4	5.4	10.0	5.6
$2600\text{-}Z\text{-}5.0\text{-}80\mathrm{k}$	4.6	9.4	4.8	4.0	7.6	4.2
$2600\text{-}Z\text{-}5.0\text{-}100\mathrm{k}$	3.8	7.8	3.9	3.4	6.3	3.5
$2600\text{-}Z\text{-}10.0\text{-}60\mathrm{k}$	12.3	24.9	12.9	10.6	19.6	11.0
$2600\text{-}Z\text{-}10.0\text{-}80\mathrm{k}$	10.1	20.4	10.5	8.7	16.0	9.0
$2600\text{-}Z\text{-}10.0\text{-}100\mathrm{k}$	8.7	17.6	9.1	7.5	13.9	7.8
2600-Y-1.0-60k	4.8	6.3	4.9	7.7	9.2	7.8
2600-Y-1.0-80k	3.0	4.0	3.1	5.0	5.9	5.0

Table A.1: continued.

	PHOENIX-ACES		BT-SETTL			
Simulation	Cond. 1	Cond. 2	Cond. 3	Cond. 1	Cond. 2	Cond. 3
2600-Y-1.0-100k	2.1	2.9	2.2	3.6	4.4	3.7
2600-Y-5.0-60k	7.2	9.1	7.3	11.7	14.2	11.9
2600-Y-5.0-80k	5.6	7.0	5.6	8.9	10.8	9.0
2600-Y-5.0-100k	4.7	5.9	4.7	7.4	9.0	7.5
2600-Y-10.0-60k	12.1	14.6	12.2	22.0	26.3	22.2
2600-Y-10.0-80k	10.1	12.2	10.2	18.0	21.6	18.3
2600-Y-10.0-100k	8.8	10.7	8.9	15.7	18.8	15.9
2600-J-1.0-60k	6.4	17.1	6.8	8.1	24.0	8.6
2600 -J- 1.0 - 80 k	4.0	10.5	4.2	5.4	16.0	5.8
2600-J-1.0-100k	2.8	7.4	3.0	4.1	12.0	4.4
$2600 ext{-}J ext{-}5.0 ext{-}60 ext{k}$	10.0	26.9	10.6	11.7	35.0	12.5
2600-J-5.0-80k	7.6	20.4	8.0	9.0	26.9	9.6
2600-J-5.0-100k	6.3	17.0	6.7	7.6	22.6	8.1
2600-J-10.0-60k	18.1	47.2	19.1	20.8	60.7	22.2
2600-J-10.0-80k	15.0	39.2	15.8	17.2	50.4	18.3
2600-J-10.0-100k	13.0	34.2	13.8	15.0	44.1	16.0
2600-H-1.0-60k	5.2	10.2	5.4	4.6	9.1	4.8
2600-H-1.0-80k	3.4	6.7	3.5	3.1	6.2	3.2
2600-H-1.0-100k	2.6	5.1	2.7	2.4	4.7	2.5
$2600 ext{-H-}5.0 ext{-}60 ext{k}$	7.8	15.4	8.0	6.8	13.5	7.0
$2600 ext{-H-}5.0 ext{-}80 ext{k}$	5.9	11.7	6.2	5.2	10.3	5.4
$2600 ext{-H-}5.0 ext{-}100 ext{k}$	5.0	9.8	5.2	4.4	8.6	4.5
$2600 ext{-H-}10.0 ext{-}60 ext{k}$	14.2	28.9	14.7	12.6	25.5	13.0
$2600 ext{-}H ext{-}10.0 ext{-}80 ext{k}$	11.7	23.8	12.1	10.3	21.0	10.7
2600-H-10.0-100k	10.2	20.7	10.6	9.0	18.3	9.4
$2600 ext{-} ext{K-}1.0 ext{-}60 ext{k}$	6.2	20.2	6.6	5.7	18.8	6.1
$2600 ext{-} ext{K-}1.0 ext{-}80 ext{k}$	4.0	13.2	4.3	3.9	12.9	4.2
$2600 ext{-} ext{K-}1.0 ext{-}100 ext{k}$	3.0	9.9	3.2	3.0	9.9	3.2
$2600 ext{-} ext{K-}5.0 ext{-}60 ext{k}$	9.4	30.1	10.0	8.3	27.2	8.9
$2600 ext{-} ext{K-}5.0 ext{-}80 ext{k}$	7.1	23.0	7.6	6.4	20.9	6.8
$2600\text{-}\mathrm{K}\text{-}5.0\text{-}100\mathrm{k}$	6.0	19.3	6.4	5.3	17.6	5.7
$2600 ext{-}10.0 ext{-}60 ext{k}$	17.4	54.0	18.6	15.2	48.5	16.2
$2600 ext{-} ext{K-}10.0 ext{-}80 ext{k}$	14.4	44.7	15.3	12.5	40.1	13.4
2600-K-10.0-100k	12.5	39.1	13.4	10.9	35.0	11.7

 $\textbf{Table A.2:} \ \ \text{RV precisions calculated for the NIRPS ETC.} \ \ \text{Reference band SELF}.$

Simulation	$\sigma_{RV}(\text{Cond. 1})$	$\sigma_{RV}(\text{Cond. 2})$	$\sigma_{RV}(\mathrm{Cond.}3)$
$(T_{\text{eff}}\text{-Band-}v.sini\text{-R})$	[m/s]	[m/s]	[m/s]
4000-Z-1.0-75k	6.9	11.2	7.1
4000-Z-1.0-100k	4.7	7.7	4.9
4000-Z-5.0-75k	11.2	18.2	11.6
4000-Z-5.0-100k	9.0	14.5	9.3
4000-Z-10.0-75k	20.5	32.6	21.1
$4000\text{-}Z\text{-}10.0\text{-}100\mathrm{k}$	17.2	27.4	17.8
4000-Y-1.0-75k	6.8	8.1	6.8
4000-Y-1.0-100k	4.4	5.2	4.4
4000-Y-5.0-75k	12.5	14.9	12.6
4000-Y-5.0-100k	9.8	11.7	9.9
4000-Y-10.0-75k	26.4	31.6	26.8
4000-Y-10.0-100k	21.9	26.2	22.2
4000-J-1.0-75k	11.3	29.3	11.9
4000-J-1.0-100k	7.8	19.7	8.2
4000-J-5.0-75k	18.1	50.1	19.1
4000-J-5.0-100k	14.5	39.7	15.3
4000-J-10.0-75k	32.3	102.4	34.3
4000-J-10.0-100k	27.2	85.5	28.9
4000-H-1.0-75k	5.4	8.5	5.5
4000-H-1.0-100k	3.9	6.2	4.0
4000-H-5.0-75k	8.2	13.0	8.4
$4000 ext{-H-}5.0 ext{-}100 ext{k}$	6.6	10.4	6.7
$4000 ext{-H-}10.0 ext{-}75 ext{k}$	15.0	23.5	15.4
$4000 ext{-H-}10.0 ext{-}100 ext{k}$	12.6	19.7	12.9
4000-K-1.0-75k	10.4	47.3	11.1
4000-K-1.0-100k	7.3	33.7	7.8
$4000 ext{-} ext{K-}5.0 ext{-}75 ext{k}$	17.2	73.5	18.4
$4000\text{-}\mathrm{K}\text{-}5.0\text{-}100\mathrm{k}$	13.7	59.0	14.6
$4000 ext{-} ext{K-}10.0 ext{-}75 ext{k}$	33.4	132.8	35.7
4000-K-10.0-100k	28.0	111.8	29.9
3900-Z-1.0-75k	7.0	11.4	7.2
3900-Z-1.0-100k	4.7	7.8	4.9
3900-Z-5.0-75k	11.5	18.6	11.9
3900-Z-5.0-100k	9.2	14.8	9.5
3900-Z-10.0-75k	21.2	33.6	21.8
3900-Z-10.0-100k	17.8	28.2	18.3
3900-Y-1.0-75k	6.6	7.9	6.7
3900-Y-1.0-100k	4.2	5.1	4.3
3900-Y-5.0-75k	12.3	14.7	12.5

Table A.2: continued.

Simulation	$\sigma_{RV}(\text{Cond. 1})$	$\sigma_{RV}(\text{Cond. 2})$	$\sigma_{RV}(\text{Cond. 3})$
3900-Y-5.0-100k	9.7	11.5	9.8
3900-Y-10.0-75k	26.3	31.4	26.6
3900-Y-10.0-100k	21.8	26.0	22.1
3900-J-1.0-75k	11.5	29.5	12.1
3900-J-1.0-100k	7.9	19.6	8.3
3900-J-5.0-75k	18.5	50.9	19.6
$3900\text{-J-}5.0\text{-}100\mathrm{k}$	14.8	40.3	15.6
$3900\text{-J-}10.0\text{-}75\mathrm{k}$	33.4	104.9	35.4
$3900\text{-J-}10.0\text{-}100\mathrm{k}$	28.0	87.6	29.8
3900-H-1.0-75k	5.4	8.6	5.5
3900-H-1.0-100k	4.0	6.3	4.0
3900-H-5.0-75k	8.3	13.0	8.5
$3900\text{-H-}5.0\text{-}100\mathrm{k}$	6.6	10.5	6.8
$3900\text{-H-}10.0\text{-}75\mathrm{k}$	15.1	23.6	15.5
$3900\text{-H-}10.0\text{-}100\mathrm{k}$	12.7	19.9	13.0
$3900\text{-}\mathrm{K}\text{-}1.0\text{-}75\mathrm{k}$	10.6	47.3	11.3
3900-K-1.0-100k	7.4	33.6	8.0
$3900\text{-}\mathrm{K}\text{-}5.0\text{-}75\mathrm{k}$	17.5	73.8	18.7
$3900\text{-}\mathrm{K}\text{-}5.0\text{-}100\mathrm{k}$	13.9	59.2	14.8
$3900\text{-}\mathrm{K}\text{-}10.0\text{-}75\mathrm{k}$	34.0	133.7	36.3
3900-K-10.0-100k	28.5	112.5	30.5
3800-Z-1.0-75k	6.9	11.3	7.2
3800-Z-1.0-100k	4.7	7.7	4.8
$3800\text{-}Z\text{-}5.0\text{-}75\mathrm{k}$	11.7	18.7	12.0
3800-Z-5.0-100k	9.3	14.9	9.6
3800-Z-10.0-75k	21.7	34.2	22.4
$3800\text{-}Z\text{-}10.0\text{-}100\mathrm{k}$	18.2	28.7	18.8
3800-Y-1.0-75k	6.5	7.7	6.5
3800-Y-1.0-100k	4.1	4.9	4.2
3800-Y-5.0-75k	12.1	14.4	12.3
3800-Y-5.0-100k	9.5	11.3	9.6
3800-Y-10.0-75k	26.0	31.0	26.3
3800-Y-10.0-100k	21.5	25.7	21.8
3800-J-1.0-75k	11.5	29.3	12.1
3800-J-1.0-100k	7.8	19.4	8.2
3800-J-5.0-75k	18.7	51.2	19.8
3800-J-5.0-100k	14.9	40.5	15.8
3800-J-10.0-75k	34.1	106.2	36.2
3800-J-10.0-100k	28.7	88.6	30.4
3800-H-1.0-75k	5.5	8.8	5.7

Table A.2: continued.

	(0 11)	(C 1.0)	(C 1.0)
Simulation	$\sigma_{RV}(\text{Cond. 1})$	$\sigma_{RV}(\text{Cond. 2})$	$\sigma_{RV}(\text{Cond. 3})$
3800-H-1.0-100k	4.1	6.4	4.1
3800-H-5.0-75k	8.4	13.2	8.6
3800-H-5.0-100k	6.7	10.6	6.9
3800-H-10.0-75k	15.2	23.7	15.6
3800-H-10.0-100k	12.8	20.0	13.1
3800-K-1.0-75k	10.7	46.0	11.4
3800-K-1.0-100k	7.5	32.5	8.0
3800-K-5.0-75k	17.7	72.6	18.9
3800-K-5.0-100k	14.0	58.2	15.0
3800-K-10.0-75k	34.4	132.6	36.7
3800-K-10.0-100k	28.8	111.5	30.8
3700-Z-1.0-75k	6.8	11.1	7.0
3700-Z-1.0-100k	4.5	7.4	4.6
3700-Z-5.0-75k	11.6	18.7	12.0
3700-Z-5.0-100k	9.2	14.8	9.5
3700-Z-10.0-75k	22.0	34.6	22.7
3700-Z-10.0-100k	18.4	29.1	19.0
3700-Y-1.0-75k	6.3	7.5	6.3
3700-Y-1.0-100k	4.0	4.8	4.0
3700-Y-5.0-75k	11.9	14.1	12.0
3700-Y-5.0-100k	9.3	11.0	9.4
3700-Y-10.0-75k	25.6	30.4	25.9
3700-Y-10.0-100k	21.2	25.2	21.4
3700-J-1.0-75k	11.4	28.8	12.0
3700-J-1.0-100k	7.7	18.9	8.1
3700 -J- 5.0 - 75 k	18.8	50.9	19.9
3700-J-5.0-100k	15.0	40.2	15.8
$3700\text{-J-}10.0\text{-}75\mathrm{k}$	34.7	106.0	36.8
$3700\text{-J-}10.0\text{-}100\mathrm{k}$	29.1	88.4	30.9
3700-H-1.0-75k	5.7	9.0	5.8
$3700\text{-H}\text{-}1.0\text{-}100\mathrm{k}$	4.2	6.6	4.3
$3700\text{-H-}5.0\text{-}75\mathrm{k}$	8.5	13.4	8.7
$3700\text{-H-}5.0\text{-}100\mathrm{k}$	6.8	10.8	7.0
$3700\text{-H-}10.0\text{-}75\mathrm{k}$	15.3	24.0	15.7
3700-H-10.0-100k	12.9	20.2	13.2
$3700\text{-}\mathrm{K}\text{-}1.0\text{-}75\mathrm{k}$	10.6	43.7	11.4
3700-K-1.0-100k	7.5	30.7	8.0
$3700\text{-}\mathrm{K}\text{-}5.0\text{-}75\mathrm{k}$	17.7	70.1	18.9
$3700\text{-}\mathrm{K}\text{-}5.0\text{-}100\mathrm{k}$	14.0	56.0	15.0
3700-K-10.0-75k	34.5	128.8	36.8

Table A.2: continued.

Simulation	$\sigma_{RV}(\text{Cond. 1})$	$\sigma_{RV}(\text{Cond. 2})$	$\sigma_{RV}(\text{Cond. 3})$
3700-K-10.0-100k	28.9	108.3	30.9
3600-Z-1.0-75k	6.3	10.5	6.6
3600-Z-1.0-100k	4.1	6.9	4.3
3600-Z-5.0-75k	11.2	18.2	11.6
$3600\text{-}Z\text{-}5.0\text{-}100\mathrm{k}$	8.9	14.4	9.2
$3600\text{-}Z\text{-}10.0\text{-}75\mathrm{k}$	21.8	34.5	22.5
$3600\text{-}Z\text{-}10.0\text{-}100\mathrm{k}$	18.2	28.9	18.8
3600-Y-1.0-75k	6.0	7.2	6.1
3600-Y-1.0-100k	3.8	4.6	3.9
3600-Y-5.0-75k	11.5	13.6	11.6
3600-Y-5.0-100k	9.0	10.6	9.1
3600-Y-10.0-75k	24.9	29.6	25.2
3600-Y-10.0-100k	20.6	24.5	20.9
$3600\text{-J-}1.0\text{-}75\mathrm{k}$	11.1	27.9	11.7
3600-J-1.0-100k	7.5	18.1	7.8
$3600\text{-J-}5.0\text{-}75\mathrm{k}$	18.7	49.8	19.7
3600-J-5.0-100k	14.8	39.3	15.7
$3600 ext{-}J ext{-}10.0 ext{-}75 ext{k}$	34.7	104.0	36.9
$3600\text{-J-}10.0\text{-}100\mathrm{k}$	29.1	86.7	30.9
3600-H-1.0-75k	5.8	9.2	5.9
$3600\text{-H-}1.0\text{-}100\mathrm{k}$	4.3	6.8	4.3
3600-H-5.0-75k	8.6	13.7	8.8
$3600 ext{-H-}5.0 ext{-}100 ext{k}$	6.9	11.0	7.1
$3600 ext{-H-}10.0 ext{-}75 ext{k}$	15.4	24.3	15.8
$3600\text{-H-}10.0\text{-}100\mathrm{k}$	13.0	20.5	13.3
$3600 ext{-} ext{K-}1.0 ext{-}75 ext{k}$	10.3	39.8	11.0
$3600\text{-}\mathrm{K}\text{-}1.0\text{-}100\mathrm{k}$	7.2	27.8	7.7
$3600\text{-}\mathrm{K}\text{-}5.0\text{-}75\mathrm{k}$	17.2	64.7	18.4
$3600\text{-}\mathrm{K}\text{-}5.0\text{-}100\mathrm{k}$	13.7	51.6	14.6
$3600\text{-}\mathrm{K}\text{-}10.0\text{-}75\mathrm{k}$	33.7	120.0	36.0
$3600\text{-}\mathrm{K}\text{-}10.0\text{-}100\mathrm{k}$	28.2	100.8	30.2
$3500\text{-}Z\text{-}1.0\text{-}75\mathrm{k}$	5.8	9.7	6.0
$3500\text{-}Z\text{-}1.0\text{-}100\mathrm{k}$	3.7	6.3	3.8
$3500\text{-}Z\text{-}5.0\text{-}75\mathrm{k}$	10.6	17.3	10.9
$3500\text{-}Z\text{-}5.0\text{-}100\mathrm{k}$	8.3	13.6	8.6
$3500\text{-}Z\text{-}10.0\text{-}75\mathrm{k}$	21.1	33.8	21.8
$3500\text{-}Z\text{-}10.0\text{-}100\mathrm{k}$	17.6	28.2	18.2
3500-Y-1.0-75k	5.8	6.9	5.8
3500-Y-1.0-100k	3.6	4.3	3.7
3500-Y-5.0-75k	11.0	13.1	11.2

Table A.2: continued.

C:1-+:	- (C1 1)	- (C1.9)	- (C1-2)
Simulation	$\sigma_{RV}(\text{Cond. 1})$	$\sigma_{RV}(\text{Cond. 2})$	$\sigma_{RV}(\text{Cond. 3})$
3500-Y-5.0-100k	8.6	10.2	8.7
3500-Y-10.0-75k	24.0	28.5	24.3
3500-Y-10.0-100k	19.9	23.6	20.1
3500-J-1.0-75k	10.7	26.6	11.3
3500-J-1.0-100k	7.1	17.1	7.5
3500-J-5.0-75k	18.3	48.1	19.3
3500-J-5.0-100k	14.5	37.8	15.3
3500-J-10.0-75k	34.4	100.5	36.5
3500-J-10.0-100k	28.8	83.7	30.6
3500-H-1.0-75k	5.8	9.4	6.0
3500-H-1.0-100k	4.3	6.9	4.4
3500-H-5.0-75k	8.8	14.0	9.0
3500-H-5.0-100k	7.1	11.3	7.2
3500-H-10.0-75k	15.6	24.8	16.0
3500-H-10.0-100k	13.1	20.9	13.5
$3500 ext{-} ext{K-}1.0 ext{-}75 ext{k}$	9.8	35.7	10.5
$3500\text{-} ext{K-}1.0\text{-}100 ext{k}$	6.8	24.8	7.3
$3500\text{-}\mathrm{K}\text{-}5.0\text{-}75\mathrm{k}$	16.4	58.2	17.5
$3500 ext{-} ext{K-}5.0 ext{-}100 ext{k}$	13.0	46.4	13.9
$3500 ext{-}10.0 ext{-}75 ext{k}$	32.2	108.7	34.4
$3500\text{-}\mathrm{K}\text{-}10.0\text{-}100\mathrm{k}$	27.0	91.3	28.8
$3400\text{-}Z\text{-}1.0\text{-}75\mathrm{k}$	5.3	8.9	5.5
$3400\text{-}Z\text{-}1.0\text{-}100\mathrm{k}$	3.3	5.7	3.5
$3400\text{-}Z\text{-}5.0\text{-}75\mathrm{k}$	9.8	16.3	10.2
$3400\text{-}Z\text{-}5.0\text{-}100\mathrm{k}$	7.7	12.8	8.0
$3400\text{-}Z\text{-}10.0\text{-}75\mathrm{k}$	20.2	32.7	20.8
$3400\text{-}Z\text{-}10.0\text{-}100\mathrm{k}$	16.8	27.2	17.3
3400-Y-1.0-75k	5.5	6.6	5.6
3400-Y-1.0-100k	3.5	4.2	3.5
3400-Y-5.0-75k	10.5	12.4	10.6
3400-Y-5.0-100k	8.2	9.7	8.3
3400-Y-10.0-75k	22.3	26.4	22.5
3400-Y-10.0-100k	18.5	21.9	18.7
$3400 ext{-}J ext{-}1.0 ext{-}75 ext{k}$	10.2	25.0	10.8
3400-J-1.0-100k	6.7	15.9	7.1
3400 -J - 5.0 - 75 k	17.6	45.6	18.6
3400-J-5.0-100k	14.0	35.9	14.7
$3400 ext{-}J ext{-}10.0 ext{-}75 ext{k}$	33.6	95.5	35.7
3400-J-10.0-100k	28.1	79.4	29.9
3400-H-1.0-75k	5.9	9.7	6.0

Table A.2: continued.

Simulation	$\sigma_{RV}(\text{Cond. 1})$	$\sigma_{RV}(\text{Cond.}2)$	$\sigma_{RV}(\text{Cond. }3)$
3400-H-1.0-100k	4.3	7.1	4.4
3400-H-5.0-75k	8.9	14.5	9.2
3400-H-5.0-100k	7.2	11.7	7.4
3400-H-10.0-75k	16.0	25.8	16.4
3400-H-10.0-100k	13.4	21.7	13.8
3400-K-1.0-75k	9.2	31.8	9.8
3400-K-1.0-100k	6.4	22.2	6.8
$3400 ext{-} ext{K-}5.0 ext{-}75 ext{k}$	15.4	52.0	16.4
3400-K-5.0-100k	12.2	41.4	13.0
3400-K-10.0-75k	30.5	97.5	32.4
3400-K-10.0-100k	25.5	81.8	27.2
$3300\text{-}Z\text{-}1.0\text{-}75\mathrm{k}$	4.8	8.2	5.0
3300-Z-1.0-100k	3.0	5.2	3.1
$3300\text{-}Z\text{-}5.0\text{-}75\mathrm{k}$	9.1	15.3	9.4
$3300\text{-}Z\text{-}5.0\text{-}100\mathrm{k}$	7.1	11.9	7.3
$3300\text{-}Z\text{-}10.0\text{-}75\mathrm{k}$	19.0	31.3	19.7
$3300\text{-}Z\text{-}10.0\text{-}100\mathrm{k}$	15.8	26.0	16.4
3300-Y-1.0-75k	5.8	7.1	5.9
3300-Y-1.0-100k	3.8	4.6	3.8
3300-Y-5.0-75k	10.3	12.2	10.4
3300-Y-5.0-100k	8.1	9.7	8.2
3300-Y-10.0-75k	19.9	23.5	20.1
3300-Y-10.0-100k	16.6	19.6	16.8
3300-J-1.0-75k	9.5	23.0	10.1
$3300\text{-J-}1.0\text{-}100\mathrm{k}$	6.2	14.6	6.6
3300-J-5.0-75k	16.7	42.5	17.7
$3300\text{-J-}5.0\text{-}100\mathrm{k}$	13.2	33.3	13.9
$3300\text{-J-}10.0\text{-}75\mathrm{k}$	32.3	89.0	34.3
$3300\text{-J-}10.0\text{-}100\mathrm{k}$	27.0	74.0	28.6
$3300 ext{-H-}1.0 ext{-}75 ext{k}$	5.9	10.0	6.1
$3300\text{-H-}1.0\text{-}100\mathrm{k}$	4.3	7.2	4.4
$3300 ext{-H-}5.0 ext{-}75 ext{k}$	9.1	15.2	9.4
$3300\text{-H-}5.0\text{-}100\mathrm{k}$	7.3	12.2	7.5
$3300\text{-H-}10.0\text{-}75\mathrm{k}$	16.5	27.3	16.9
$3300\text{-H}\text{-}10.0\text{-}100\mathrm{k}$	13.9	22.9	14.2
$3300\text{-}\mathrm{K}\text{-}1.0\text{-}75\mathrm{k}$	8.7	28.9	9.2
$3300\text{-}\mathrm{K}\text{-}1.0\text{-}100\mathrm{k}$	6.0	20.2	6.4
$3300 ext{-} ext{K-}5.0 ext{-}75 ext{k}$	14.6	47.2	15.5
$3300\text{-}\mathrm{K}\text{-}5.0\text{-}100\mathrm{k}$	11.5	37.6	12.3
3300-K-10.0-75k	28.8	88.8	30.7

Table A.2: continued.

Simulation	$\sigma_{RV}(\text{Cond. 1})$	$\sigma_{RV}(\mathrm{Cond.}2)$	$\sigma_{RV}(\mathrm{Cond.}3)$
3300-K-10.0-100k	24.1	74.6	25.7
$3200\text{-}Z\text{-}1.0\text{-}75\mathrm{k}$	4.3	7.5	4.5
$3200\text{-}Z\text{-}1.0\text{-}100\mathrm{k}$	2.7	4.7	2.8
$3200\text{-}Z\text{-}5.0\text{-}75\mathrm{k}$	8.3	14.2	8.6
$3200\text{-}Z\text{-}5.0\text{-}100\mathrm{k}$	6.5	11.1	6.7
$3200\text{-}Z\text{-}10.0\text{-}75\mathrm{k}$	17.8	29.8	18.4
$3200\text{-}Z\text{-}10.0\text{-}100\mathrm{k}$	14.7	24.7	15.3
3200-Y-1.0-75k	5.5	6.7	5.6
3200-Y-1.0-100k	3.6	4.4	3.6
3200-Y-5.0-75k	9.7	11.6	9.8
$3200\text{-}Y\text{-}5.0\text{-}100\mathrm{k}$	7.6	9.2	7.7
3200-Y-10.0-75k	18.4	21.7	18.6
$3200\text{-}\mathrm{Y}\text{-}10.0\text{-}100\mathrm{k}$	15.4	18.2	15.6
$3200\text{-J-}1.0\text{-}75\mathrm{k}$	8.7	20.6	9.2
$3200\text{-J-}1.0\text{-}100\mathrm{k}$	5.6	13.0	5.9
3200 -J- 5.0 - 75 k	15.5	38.5	16.3
$3200\text{-J-}5.0\text{-}100\mathrm{k}$	12.2	30.2	12.9
$3200\text{-J-}10.0\text{-}75\mathrm{k}$	30.3	80.8	32.1
$3200\text{-J-}10.0\text{-}100\mathrm{k}$	25.3	67.2	26.8
$3200\text{-H-}1.0\text{-}75\mathrm{k}$	5.9	10.3	6.1
$3200\text{-H-}1.0\text{-}100\mathrm{k}$	4.2	7.4	4.3
$3200 ext{-H-}5.0 ext{-}75 ext{k}$	9.3	15.9	9.6
$3200 ext{-H-}5.0 ext{-}100 ext{k}$	7.4	12.7	7.7
$3200\text{-H-}10.0\text{-}75\mathrm{k}$	17.0	29.0	17.5
$3200\text{-H-}10.0\text{-}100\mathrm{k}$	14.3	24.4	14.7
$3200\text{-}\mathrm{K}\text{-}1.0\text{-}75\mathrm{k}$	8.2	26.9	8.7
$3200\text{-}\mathrm{K}\text{-}1.0\text{-}100\mathrm{k}$	5.7	18.8	6.1
$3200\text{-}\mathrm{K}\text{-}5.0\text{-}75\mathrm{k}$	13.8	43.9	14.7
$3200\text{-}\mathrm{K}\text{-}5.0\text{-}100\mathrm{k}$	10.9	34.9	11.6
$3200\text{-}\mathrm{K}\text{-}10.0\text{-}75\mathrm{k}$	27.4	82.7	29.2
$3200\text{-}\mathrm{K}\text{-}10.0\text{-}100\mathrm{k}$	22.9	69.4	24.4
$3100\text{-}Z\text{-}1.0\text{-}75\mathrm{k}$	4.0	7.3	4.2
$3100\text{-}Z\text{-}1.0\text{-}100\mathrm{k}$	2.5	4.6	2.6
3100-Z-5.0-75k	7.8	13.8	8.1
$3100\text{-}Z\text{-}5.0\text{-}100\mathrm{k}$	6.1	10.8	6.3
$3100\text{-}Z\text{-}10.0\text{-}75\mathrm{k}$	16.7	29.0	17.3
$3100\text{-}Z\text{-}10.0\text{-}100\mathrm{k}$	13.9	24.1	14.4
3100-Y-1.0-75k	5.5	6.8	5.6
3100-Y-1.0-100k	3.6	4.5	3.7
3100-Y-5.0-75k	9.4	11.3	9.5

Table A.2: continued.

Simulation	$\sigma_{RV}(\text{Cond. 1})$	$\sigma_{RV}(\text{Cond.}2)$	$\sigma_{RV}(\text{Cond. 3})$
3100-Y-5.0-100k	7.5	9.0	7.5
3100-Y-10.0-75k	17.3	20.5	17.5
3100-Y-10.0-100k	14.5	17.2	14.7
3100-J-1.0-75k	7.7	17.9	8.1
3100-J-1.0-100k	5.0	11.2	5.2
3100-J-5.0-75k	13.9	34.0	14.7
3100-J-5.0-100k	11.0	26.6	11.6
3100-J-10.0-75k	27.7	71.5	29.3
3100-J-10.0-100k	23.1	59.4	24.4
3100-H-1.0-75k	5.8	10.4	6.0
3100-H-1.0-100k	4.1	7.4	4.3
3100-H-5.0-75k	9.3	16.4	9.6
3100-H-5.0-100k	7.4	13.1	7.7
3100-H-10.0-75k	17.3	30.6	17.9
3100-H-10.0-100k	14.5	25.6	15.0
3100-K-1.0-75k	7.7	25.2	8.2
3100-K-1.0-100k	5.4	17.6	5.7
$3100 ext{-} ext{K-}5.0 ext{-}75 ext{k}$	13.1	41.3	13.9
3100-K-5.0-100k	10.3	32.8	11.0
$3100 ext{-} ext{K-}10.0 ext{-}75 ext{k}$	26.0	77.9	27.7
$3100\text{-}\mathrm{K}\text{-}10.0\text{-}100\mathrm{k}$	21.7	65.4	23.1
3000-Z-1.0-75k	3.6	6.8	3.8
3000-Z-1.0-100k	2.3	4.2	2.4
$3000\text{-}Z\text{-}5.0\text{-}75\mathrm{k}$	7.1	12.9	7.4
$3000\text{-}Z\text{-}5.0\text{-}100\mathrm{k}$	5.5	10.0	5.7
$3000\text{-}Z\text{-}10.0\text{-}75\mathrm{k}$	15.3	27.1	15.9
$3000\text{-}Z\text{-}10.0\text{-}100\mathrm{k}$	12.7	22.5	13.2
3000-Y-1.0-75k	5.0	6.3	5.1
3000-Y-1.0-100k	3.3	4.2	3.4
3000-Y-5.0-75k	8.6	10.4	8.7
3000-Y-5.0-100k	6.8	8.3	6.9
3000-Y-10.0-75k	15.7	18.6	15.9
3000-Y-10.0-100k	13.2	15.7	13.3
3000-J-1.0-75k	7.9	20.4	8.3
3000-J-1.0-100k	5.1	13.1	5.4
$3000 ext{-J-}5.0 ext{-}75 ext{k}$	13.9	37.0	14.7
3000-J-5.0-100k	11.0	29.1	11.6
$3000\text{-J-}10.0\text{-}75\mathrm{k}$	26.7	72.6	28.3
3000-J-10.0-100k	22.3	60.8	23.7
3000-H-1.0-75k	5.6	10.3	5.8

Table A.2: continued.

Simulation	$\sigma_{RV}(\text{Cond. 1})$	$\sigma_{RV}(\text{Cond. 2})$	$\sigma_{RV}(\text{Cond. 3})$
3000-H-1.0-100k	3.9	7.3	4.1
3000-H-5.0-75k	9.1	16.5	9.4
3000-H-5.0-100k	7.2	13.2	7.5
3000-H-10.0-75k	17.2	31.4	17.8
3000-H-10.0-100k	14.4	26.3	14.9
3000-K-1.0-75k	7.2	23.5	7.7
3000-K-1.0-100k	5.0	16.4	5.3
3000-K-5.0-75k	12.2	38.6	13.0
$3000\text{-}\mathrm{K}\text{-}5.0\text{-}100\mathrm{k}$	9.6	30.7	10.2
$3000\text{-}\mathrm{K}\text{-}10.0\text{-}75\mathrm{k}$	24.2	73.0	25.8
$3000\text{-}\mathrm{K}\text{-}10.0\text{-}100\mathrm{k}$	20.3	61.2	21.6
$2900\text{-}Z\text{-}1.0\text{-}75\mathrm{k}$	3.3	6.2	3.4
2900-Z-1.0-100k	2.0	3.9	2.1
2900-Z-5.0-75k	6.4	11.8	6.6
2900-Z-5.0-100k	4.9	9.2	5.1
2900-Z-10.0-75k	13.8	25.1	14.4
$2900\text{-}Z\text{-}10.0\text{-}100\mathrm{k}$	11.4	20.8	11.9
2900-Y-1.0-75k	4.6	5.8	4.6
2900-Y-1.0-100k	3.0	3.9	3.0
2900-Y-5.0-75k	7.8	9.6	7.9
2900-Y-5.0-100k	6.2	7.6	6.3
2900-Y-10.0-75k	14.2	16.8	14.3
2900-Y-10.0-100k	11.9	14.2	12.0
$2900\text{-J-}1.0\text{-}75\mathrm{k}$	7.1	18.6	7.5
2900-J-1.0-100k	4.6	12.0	4.9
$2900\text{-J-}5.0\text{-}75\mathrm{k}$	12.5	33.5	13.3
2900-J-5.0-100k	9.9	26.4	10.5
$2900\text{-J-}10.0\text{-}75\mathrm{k}$	24.0	64.3	25.5
2900-J-10.0-100k	20.1	53.9	21.3
2900-H-1.0-75k	5.3	9.9	5.4
2900-H-1.0-100k	3.7	6.9	3.8
2900-H-5.0-75k	8.6	16.1	8.9
2900-H-5.0-100k	6.9	12.8	7.1
2900-H-10.0-75k	16.5	31.2	17.1
2900-H-10.0-100k	13.8	26.1	14.3
2900-K-1.0-75k	6.6	21.6	7.0
2900-K-1.0-100k	4.5	15.0	4.8
2900-K-5.0-75k	11.1	35.5	11.8
2900-K-5.0-100k	8.8	28.3	9.4
$2900\text{-}\mathrm{K}\text{-}10.0\text{-}75\mathrm{k}$	22.1	67.3	23.6

Table A.2: continued.

G: 1	(C 1.1)	(C 1.9)	(C 1.2)
Simulation	$\sigma_{RV}(\text{Cond. 1})$	$\sigma_{RV}(\text{Cond. 2})$	$\sigma_{RV}(\text{Cond. 3})$
2900-K-10.0-100k	18.5	56.5	19.7
2800-Z-1.0-75k	2.9	5.7	3.0
2800-Z-1.0-100k	1.8	3.6	1.9
2800-Z-5.0-75k	5.7	10.9	5.9
2800-Z-5.0-100k	4.4	8.5	4.6
2800-Z-10.0-75k	12.4	23.3	13.0
2800-Z-10.0-100k	10.3	19.3	10.7
2800-Y-1.0-75k	4.1	5.3	4.2
2800-Y-1.0-100k	2.7	3.5	2.7
2800-Y-5.0-75k	7.1	8.7	7.2
2800-Y-5.0-100k	5.6	7.0	5.7
2800-Y-10.0-75k	12.7	15.2	12.9
2800-Y-10.0-100k	10.7	12.8	10.8
2800-J-1.0-75k	6.1	16.0	6.5
2800-J-1.0-100k	4.0	10.2	4.2
2800-J-5.0-75k	10.9	28.9	11.5
2800-J-5.0-100k	8.6	22.8	9.1
2800-J-10.0-75k	20.9	55.0	22.1
2800-J-10.0-100k	17.5	46.1	18.5
2800-H-1.0-75k	4.8	9.3	5.0
2800-H-1.0-100k	3.3	6.4	3.5
$2800 ext{-H-}5.0 ext{-}75 ext{k}$	8.0	15.3	8.2
2800-H-5.0-100k	6.3	12.1	6.5
$2800 ext{-H-}10.0 ext{-}75 ext{k}$	15.3	29.9	15.9
2800-H-10.0-100k	12.8	25.0	13.3
$2800 ext{-} ext{K-}1.0 ext{-}75 ext{k}$	5.9	19.5	6.3
$2800\text{-}\mathrm{K}\text{-}1.0\text{-}100\mathrm{k}$	4.0	13.5	4.3
$2800 ext{-} ext{K-}5.0 ext{-}75 ext{k}$	10.0	32.2	10.6
$2800\text{-}\mathrm{K}\text{-}5.0\text{-}100\mathrm{k}$	7.9	25.6	8.4
$2800\text{-}\mathrm{K}\text{-}10.0\text{-}75\mathrm{k}$	19.8	60.9	21.1
$2800\text{-}\mathrm{K}\text{-}10.0\text{-}100\mathrm{k}$	16.6	51.1	17.7
$2700\text{-}Z\text{-}1.0\text{-}75\mathrm{k}$	2.6	5.3	2.7
$2700\text{-}Z\text{-}1.0\text{-}100\mathrm{k}$	1.6	3.3	1.7
$2700\text{-}Z\text{-}5.0\text{-}75\mathrm{k}$	5.2	10.2	5.4
$2700\text{-}Z\text{-}5.0\text{-}100\mathrm{k}$	4.0	7.9	4.2
2700-Z-10.0-75k	11.3	21.9	11.8
$2700\text{-}Z\text{-}10.0\text{-}100\mathrm{k}$	9.3	18.1	9.7
2700-Y-1.0-75k	3.7	4.8	3.7
2700-Y-1.0-100k	2.4	3.2	2.4
2700-Y-5.0-75k	6.4	8.0	6.5

Table A.2: continued.

Simulation	$\sigma_{RV}(\text{Cond. 1})$	$\sigma_{RV}(\text{Cond. 2})$	$\sigma_{RV}(\text{Cond. 3})$
2700-Y-5.0-100k	5.1	6.4	5.2
2700-Y-10.0-75k	11.5	13.8	11.6
2700-Y-10.0-100k	9.7	11.6	9.8
2700-J-1.0-75k	5.2	13.6	5.5
2700-J-1.0-100k	3.4	8.7	3.5
2700-J-5.0-75k	9.3	24.9	9.9
2700-J-5.0-100k	7.4	19.6	7.8
$2700\text{-J-}10.0\text{-}75\mathrm{k}$	18.0	47.1	19.1
2700-J-10.0-100k	15.1	39.5	16.0
2700-H-1.0-75k	4.3	8.3	4.4
2700-H-1.0-100k	3.0	5.8	3.1
$2700 ext{-H-}5.0 ext{-}75 ext{k}$	7.1	13.9	7.4
$2700 ext{-H-}5.0 ext{-}100 ext{k}$	5.7	11.0	5.9
2700-H-10.0-75k	13.8	27.6	14.3
$2700\text{-H-}10.0\text{-}100\mathrm{k}$	11.5	23.1	12.0
$2700 ext{-} ext{K-}1.0 ext{-}75 ext{k}$	5.2	17.2	5.5
2700-K-1.0-100k	3.5	11.9	3.8
$2700 ext{-} ext{K-}5.0 ext{-}75 ext{k}$	8.8	28.5	9.4
$2700 ext{-} ext{K-}5.0 ext{-}100 ext{k}$	6.9	22.7	7.4
$2700 ext{-}10.0 ext{-}75 ext{k}$	17.4	54.0	18.6
$2700\text{-}\mathrm{K}\text{-}10.0\text{-}100\mathrm{k}$	14.6	45.3	15.5
$2600\text{-}Z\text{-}1.0\text{-}75\mathrm{k}$	2.5	5.2	2.6
$2600\text{-}Z\text{-}1.0\text{-}100\mathrm{k}$	1.5	3.2	1.6
$2600\text{-}Z\text{-}5.0\text{-}75\mathrm{k}$	4.8	9.9	5.1
$2600\text{-}Z\text{-}5.0\text{-}100\mathrm{k}$	3.8	7.8	3.9
$2600\text{-}Z\text{-}10.0\text{-}75\mathrm{k}$	10.5	21.3	11.0
$2600\text{-}Z\text{-}10.0\text{-}100\mathrm{k}$	8.7	17.6	9.1
2600-Y-1.0-75k	3.3	4.4	3.4
2600-Y-1.0-100k	2.1	2.9	2.2
2600-Y-5.0-75k	5.9	7.4	6.0
2600-Y-5.0-100k	4.7	5.9	4.7
2600-Y-10.0-75k	10.5	12.7	10.6
2600-Y-10.0-100k	8.8	10.7	8.9
$2600 ext{-}J ext{-}1.0 ext{-}75 ext{k}$	4.4	11.7	4.7
2600-J-1.0-100k	2.8	7.4	3.0
$2600\text{-J-}5.0\text{-}75\mathrm{k}$	8.0	21.6	8.5
$2600\text{-J-}5.0\text{-}100\mathrm{k}$	6.3	17.0	6.7
$2600 ext{-}J ext{-}10.0 ext{-}75 ext{k}$	15.6	40.8	16.5
2600-J-10.0-100k	13.0	34.2	13.8
2600-H-1.0-75k	3.7	7.4	3.9

Table A.2: continued.

Simulation	$\sigma_{RV}(\text{Cond. 1})$	$\sigma_{RV}(\text{Cond.}2)$	$\sigma_{RV}(\text{Cond. 3})$
2600-H-1.0-100k	2.6	5.1	2.7
2600-H-5.0-75k	6.3	12.4	6.5
2600-H-5.0-100k	5.0	9.8	5.2
2600-H-10.0-75k	12.2	24.8	12.7
2600-H-10.0-100k	10.2	20.7	10.6
2600-K-1.0-75k	4.4	14.4	4.7
2600-K-1.0-100k	3.0	9.9	3.2
2600-K-5.0-75k	7.6	24.3	8.1
2600-K-5.0-100k	6.0	19.3	6.4
2600-K-10.0-75k	15.0	46.5	16.0
2600-K-10.0-100k	12.5	39.1	13.4
2500-Z-1.0-75k	2.5	5.5	2.6
2500-Z-1.0-100k	1.6	3.5	1.6
2500-Z-5.0-75k	4.8	10.4	5.0
2500-Z-5.0-100k	3.7	8.2	3.9
$2500\text{-}Z\text{-}10.0\text{-}75\mathrm{k}$	10.3	22.0	10.9
2500-Z-10.0-100k	8.6	18.3	9.0
2500-Y-1.0-75k	3.1	4.2	3.1
2500-Y-1.0-100k	2.0	2.7	2.0
2500-Y-5.0-75k	5.5	7.1	5.6
2500-Y-5.0-100k	4.4	5.7	4.4
2500-Y-10.0-75k	9.9	12.2	10.0
2500-Y-10.0-100k	8.4	10.3	8.5
2500-J-1.0-75k	3.7	10.0	3.9
2500-J-1.0-100k	2.4	6.3	2.5
2500-J-5.0-75k	6.8	18.7	7.3
$2500\text{-J-}5.0\text{-}100\mathrm{k}$	5.4	14.7	5.7
$2500\text{-J-}10.0\text{-}75\mathrm{k}$	13.5	35.7	14.3
$2500\text{-J-}10.0\text{-}100\mathrm{k}$	11.3	29.9	11.9
$2500 ext{-H-}1.0 ext{-}75 ext{k}$	3.3	6.5	3.4
$2500 ext{-H-}1.0 ext{-}100 ext{k}$	2.3	4.4	2.4
$2500 ext{-H-}5.0 ext{-}75 ext{k}$	5.5	11.0	5.7
$2500 ext{-H-}5.0 ext{-}100 ext{k}$	4.4	8.7	4.5
$2500 ext{-H-}10.0 ext{-}75 ext{k}$	10.7	21.9	11.1
2500-H-10.0-100k	9.0	18.3	9.3
$2500 ext{-} ext{K-}1.0 ext{-}75 ext{k}$	3.8	11.8	4.0
$2500\text{-}\mathrm{K}\text{-}1.0\text{-}100\mathrm{k}$	2.6	8.0	2.7
$2500 ext{-} ext{K-}5.0 ext{-}75 ext{k}$	6.5	20.5	6.9
$2500\text{-}\mathrm{K}\text{-}5.0\text{-}100\mathrm{k}$	5.1	16.2	5.5
2500-K-10.0-75k	12.8	39.8	13.7

Table A.2: continued.

Simulation	$\sigma_{RV}(\mathrm{Cond.}1)$	$\sigma_{RV}(\mathrm{Cond.}2)$	$\sigma_{RV}(\text{Cond. 3})$
2500-K-10.0-100k	10.8	33.4	11.5

Table A.3: RV precisions calculated for the SPIRou ETC. Same simulations as Table A.1 but with the SNR relative to the centre of each individual band.

Simulation	$\sigma_{RV}(\text{Cond. 1})$	$\sigma_{RV}(\text{Cond.}2)$	$\sigma_{RV}(\text{Cond. 3})$
$(T_{\text{eff}}\text{-Band-}v.sini\text{-R})$	[m/s]	[m/s]	[m/s]
3900-Z-1.0-60k	9.9	16.0	10.3
3900-Z-1.0-80k	6.6	10.7	6.8
3900-Z-1.0-100k	4.9	8.1	5.1
3900-Z-5.0-60k	14.5	23.2	15.0
3900-Z-5.0-80k	11.2	18.0	11.6
3900-Z-5.0-100k	9.4	15.2	9.7
$3900\text{-}Z\text{-}10.0\text{-}60\mathrm{k}$	25.0	39.4	25.8
3900-Z-10.0-80k	20.7	32.9	21.4
$3900\text{-}Z\text{-}10.0\text{-}100\mathrm{k}$	18.1	28.8	18.7
3900-Y-1.0-60k	10.0	11.9	10.1
3900-Y-1.0-80k	6.2	7.4	6.3
3900-Y-1.0-100k	4.4	5.3	4.5
3900-Y-5.0-60k	15.9	19.0	16.1
3900-Y-5.0-80k	12.0	14.3	12.1
3900-Y-5.0-100k	10.0	11.8	10.1
3900-Y-10.0-60k	31.6	37.8	32.0
3900-Y-10.0-80k	25.8	30.8	26.1
3900-Y-10.0-100k	22.4	26.7	22.6
$3900\text{-J-}1.0\text{-}60\mathrm{k}$	15.7	41.7	16.6
$3900\text{-J-}1.0\text{-}80\mathrm{k}$	10.5	26.9	11.0
$3900\text{-J-}1.0\text{-}100\mathrm{k}$	7.9	19.6	8.3
$3900\text{-J-}5.0\text{-}60\mathrm{k}$	22.7	63.6	24.0
$3900\text{-J-}5.0\text{-}80\mathrm{k}$	17.5	48.1	18.5
$3900\text{-J-}5.0\text{-}100\mathrm{k}$	14.8	40.3	15.6
3900-J-10.0-60k	38.6	122.9	41.0
3900-J-10.0-80k	32.0	100.7	34.0
$3900\text{-J-}10.0\text{-}100\mathrm{k}$	28.0	87.6	29.8
$3900\text{-H}\text{-}1.0\text{-}60\mathrm{k}$	7.3	11.5	7.4
$3900\text{-H}\text{-}1.0\text{-}80\mathrm{k}$	5.1	8.1	5.2
$3900\text{-H-}1.0\text{-}100\mathrm{k}$	4.0	6.4	4.1
$3900\text{-H-}5.0\text{-}60\mathrm{k}$	10.2	16.0	10.4
$3900\text{-H-}5.0\text{-}80\mathrm{k}$	7.9	12.5	8.1
3900-H-5.0-100k	6.7	10.5	6.8

Table A.3: continued.

Simulation	$\sigma_{RV}(\text{Cond. 1})$	$\sigma_{RV}(\text{Cond.}2)$	$\sigma_{RV}(\text{Cond. 3})$
3900-H-10.0-60k	17.5	27.3	17.9
3900-H-10.0-80k	14.5	22.7	14.8
3900-H-10.0-100k	12.7	19.8	13.0
3900-K-1.0-60k	10.5	46.3	11.3
3900-K-1.0-80k	7.1	31.8	7.6
3900-K-1.0-100k	5.4	24.5	5.8
3900-K-5.0-60k	15.7	65.4	16.8
$3900\text{-} ext{K-}5.0\text{-}80 ext{k}$	12.0	50.8	12.8
3900-K-5.0-100k	10.1	42.9	10.8
3900-K-10.0-60k	28.5	112.6	30.4
3900-K-10.0-80k	23.6	93.1	25.2
3900-K-10.0-100k	20.6	81.2	22.0
$3500\text{-}Z\text{-}1.0\text{-}60\mathrm{k}$	8.3	13.7	8.6
$3500\text{-}Z\text{-}1.0\text{-}80\mathrm{k}$	5.2	8.7	5.4
$3500\text{-}Z\text{-}1.0\text{-}100\mathrm{k}$	3.7	6.3	3.8
$3500\text{-}Z\text{-}5.0\text{-}60\mathrm{k}$	12.9	20.9	13.3
$3500\text{-}Z\text{-}5.0\text{-}80\mathrm{k}$	9.8	16.0	10.1
$3500\text{-}Z\text{-}5.0\text{-}100\mathrm{k}$	8.2	13.4	8.5
$3500\text{-}Z\text{-}10.0\text{-}60\mathrm{k}$	24.0	38.1	24.8
$3500\text{-}Z\text{-}10.0\text{-}80\mathrm{k}$	19.7	31.5	20.4
$3500\text{-}Z\text{-}10.0\text{-}100\mathrm{k}$	17.2	27.5	17.7
3500-Y-1.0-60k	8.7	10.3	8.8
3500-Y-1.0-80k	5.3	6.3	5.4
3500-Y-1.0-100k	3.7	4.5	3.8
3500-Y-5.0-60k	14.1	16.7	14.3
3500-Y-5.0-80k	10.6	12.5	10.7
3500-Y-5.0-100k	8.8	10.4	8.9
3500-Y-10.0-60k	28.5	33.9	28.8
3500-Y-10.0-80k	23.2	27.6	23.5
3500-Y-10.0-100k	20.1	23.9	20.3
3500-J-1.0-60k	15.1	38.4	15.9
3500-J-1.0-80k	9.8	24.0	10.3
$3500\text{-J-}1.0\text{-}100\mathrm{k}$	7.1	17.1	7.5
$3500\text{-J-}5.0\text{-}60\mathrm{k}$	22.5	60.2	23.8
$3500\text{-J-}5.0\text{-}80\mathrm{k}$	17.3	45.4	18.3
$3500\text{-J-}5.0\text{-}100\mathrm{k}$	14.5	37.8	15.3
3500-J-10.0-60k	39.9	117.8	42.4
$3500\text{-J-}10.0\text{-}80\mathrm{k}$	33.0	96.4	35.1
$3500\text{-J-}10.0\text{-}100\mathrm{k}$	28.8	83.7	30.6
3500-H-1.0-60k	7.6	12.2	7.8

Table A.3: continued.

	(0 11)	(0 10)	(G 1.0)
Simulation	$\sigma_{RV}(\text{Cond. 1})$	$\sigma_{RV}(\mathrm{Cond.}2)$	$\sigma_{RV}(\text{Cond. 3})$
3500-H-1.0-80k	5.4	8.7	5.5
3500-H-1.0-100k	4.2	6.9	4.3
3500-H-5.0-60k	10.5	16.7	10.7
3500-H-5.0-80k	8.2	13.1	8.4
3500-H-5.0-100k	6.9	11.1	7.1
3500-H-10.0-60k	17.6	28.0	18.1
3500-H-10.0-80k	14.6	23.3	15.0
3500-H-10.0-100k	12.8	20.4	13.1
3500-K-1.0-60k	9.9	35.8	10.6
3500-K-1.0-80k	6.6	24.0	7.0
3500-K-1.0-100k	5.0	18.2	5.3
$3500\text{-} ext{K-}5.0\text{-}60 ext{k}$	14.8	52.3	15.8
$3500\text{-}\mathrm{K}\text{-}5.0\text{-}80\mathrm{k}$	11.3	40.2	12.1
$3500 ext{-} ext{K-}5.0 ext{-}100 ext{k}$	9.5	33.8	10.1
$3500 ext{-}10.0 ext{-}60 ext{k}$	27.2	92.1	29.1
$3500\text{-}\mathrm{K}\text{-}10.0\text{-}80\mathrm{k}$	22.5	76.0	24.0
$3500\text{-}\mathrm{K}\text{-}10.0\text{-}100\mathrm{k}$	19.6	66.3	20.9
$2800\text{-}Z\text{-}1.0\text{-}60\mathrm{k}$	3.8	7.3	3.9
$2800\text{-}Z\text{-}1.0\text{-}80\mathrm{k}$	2.3	4.5	2.4
2800-Z-1.0-100k	1.6	3.2	1.7
$2800\text{-}Z\text{-}5.0\text{-}60\mathrm{k}$	6.1	11.6	6.4
$2800\text{-}Z\text{-}5.0\text{-}80\mathrm{k}$	4.6	8.8	4.8
$2800\text{-}Z\text{-}5.0\text{-}100\mathrm{k}$	3.8	7.3	4.0
$2800\text{-}Z\text{-}10.0\text{-}60\mathrm{k}$	12.2	22.8	12.7
$2800\text{-}Z\text{-}10.0\text{-}80\mathrm{k}$	9.9	18.7	10.4
$2800\text{-}Z\text{-}10.0\text{-}100\mathrm{k}$	8.6	16.2	9.0
2800-Y-1.0-60k	5.6	7.1	5.7
2800-Y-1.0-80k	3.6	4.7	3.7
2800-Y-1.0-100k	2.6	3.4	2.7
2800-Y-5.0-60k	8.3	10.1	8.4
2800-Y-5.0-80k	6.4	7.9	6.5
2800-Y-5.0-100k	5.4	6.7	5.5
2800-Y-10.0-60k	13.8	16.4	13.9
2800-Y-10.0-80k	11.4	13.7	11.6
2800-Y-10.0-100k	10.0	12.0	10.1
2800-J-1.0-60k	8.8	23.2	9.3
2800-J-1.0-80k	5.5	14.4	5.8
2800-J-1.0-100k	4.0	10.2	4.2
2800-J-5.0-60k	13.5	35.9	14.3
2800-J-5.0-80k	10.3	27.3	10.9

Table A.3: continued.

Simulation	$\sigma_{RV}(\text{Cond. 1})$	$\sigma_{RV}(\text{Cond.}2)$	$\sigma_{RV}(\text{Cond. 3})$
2800-J-5.0-100k	8.6	22.8	9.1
2800-J-10.0-60k	24.3	63.8	25.7
2800-J-10.0-80k	20.1	52.9	21.2
2800-J-10.0-100k	17.5	46.1	18.5
2800-H-1.0-60k	6.5	12.6	6.8
2800-H-1.0-80k	4.4	8.5	4.6
2800-H-1.0-100k	3.3	6.4	3.5
2800-H-5.0-60k	9.6	18.3	9.9
$2800 ext{-H-}5.0 ext{-}80 ext{k}$	7.3	14.1	7.6
$2800 ext{-H-}5.0 ext{-}100 ext{k}$	6.2	11.8	6.4
2800-H-10.0-60k	17.2	33.5	17.8
2800-H-10.0-80k	14.2	27.6	14.7
$2800 ext{-H-}10.0 ext{-}100 ext{k}$	12.4	24.1	12.8
$2800\text{-}\mathrm{K}\text{-}1.0\text{-}60\mathrm{k}$	6.3	20.8	6.7
$2800\text{-}\mathrm{K}\text{-}1.0\text{-}80\mathrm{k}$	4.2	13.9	4.5
$2800\text{-}\mathrm{K}\text{-}1.0\text{-}100\mathrm{k}$	3.1	10.5	3.4
$2800 ext{-}5.0 ext{-}60 ext{k}$	9.5	30.4	10.1
$2800 ext{-}6.0 ext{-}80 ext{k}$	7.2	23.3	7.7
$2800\text{-}\mathrm{K}\text{-}5.0\text{-}100\mathrm{k}$	6.0	19.6	6.4
$2800\text{-}\mathrm{K}\text{-}10.0\text{-}60\mathrm{k}$	17.5	53.7	18.7
$2800\text{-}\mathrm{K}\text{-}10.0\text{-}80\mathrm{k}$	14.4	44.4	15.4
$2800\text{-}\mathrm{K}\text{-}10.0\text{-}100\mathrm{k}$	12.6	38.8	13.4
$2600\text{-}Z\text{-}1.0\text{-}60\mathrm{k}$	3.0	6.2	3.1
$2600\text{-}Z\text{-}1.0\text{-}80\mathrm{k}$	1.8	3.8	1.9
$2600\text{-}Z\text{-}1.0\text{-}100\mathrm{k}$	1.3	2.7	1.4
$2600\text{-}Z\text{-}5.0\text{-}60\mathrm{k}$	4.8	9.8	5.0
$2600\text{-}Z\text{-}5.0\text{-}80\mathrm{k}$	3.6	7.4	3.8
$2600\text{-}Z\text{-}5.0\text{-}100\mathrm{k}$	3.0	6.2	3.2
$2600\text{-}Z\text{-}10.0\text{-}60\mathrm{k}$	9.5	19.2	9.9
$2600\text{-}Z\text{-}10.0\text{-}80\mathrm{k}$	7.7	15.7	8.1
$2600\text{-}Z\text{-}10.0\text{-}100\mathrm{k}$	6.7	13.6	7.1
2600-Y-1.0-60k	4.4	5.8	4.5
2600-Y-1.0-80k	2.8	3.8	2.9
2600-Y-1.0-100k	2.0	2.7	2.1
2600-Y-5.0-60k	6.5	8.2	6.6
2600-Y-5.0-80k	5.1	6.4	5.1
2600-Y-5.0-100k	4.3	5.4	4.3
2600-Y-10.0-60k	10.7	12.9	10.8
2600-Y-10.0-80k	8.9	10.8	9.0
2600-Y-10.0-100k	7.8	9.5	7.9

Table A.3: continued.

2600-J-1.0-60k 2600-J-1.0-80k 2600-J-1.0-100k 2600-J-5.0-60k 2600-J-5.0-80k 2600-J-5.0-100k	6.4 4.0 2.8 10.0 7.6 6.3	17.1 10.5 7.4 26.9 20.4	6.8 4.2 3.0 10.6 8.0
2600-J-1.0-100k 2600-J-5.0-60k 2600-J-5.0-80k	2.8 10.0 7.6 6.3	7.4 26.9 20.4	3.0 10.6
2600-J-5.0-60k 2600-J-5.0-80k	10.0 7.6 6.3	26.9 20.4	10.6
$2600 ext{-}J ext{-}5.0 ext{-}80 ext{k}$	7.6 6.3	20.4	
	6.3		8.0
2600-J-5.0-100k			0.0
	10.1	17.0	6.7
2600-J-10.0-60k	18.1	47.2	19.1
2600-J-10.0-80k	15.0	39.2	15.8
2600-J-10.0-100k	13.0	34.2	13.8
$2600 ext{-H-}1.0 ext{-}60 ext{k}$	5.2	10.3	5.4
$2600 ext{-H-}1.0 ext{-}80 ext{k}$	3.5	6.9	3.6
$2600 ext{-H-}1.0 ext{-}100 ext{k}$	2.7	5.2	2.8
$2600 ext{-H-}5.0 ext{-}60 ext{k}$	7.7	15.3	8.0
$2600 ext{-H-}5.0 ext{-}80 ext{k}$	5.9	11.7	6.1
$2600 ext{-H-}5.0 ext{-}100 ext{k}$	5.0	9.8	5.2
$2600 ext{-H-}10.0 ext{-}60 ext{k}$	13.9	28.4	14.5
$2600 ext{-H-}10.0 ext{-}80 ext{k}$	11.5	23.3	11.9
2600-H-10.0-100k	10.0	20.4	10.4
$2600 ext{-} ext{K-}1.0 ext{-}60 ext{k}$	5.0	16.2	5.3
$2600 ext{-} ext{K-}1.0 ext{-}80 ext{k}$	3.3	10.7	3.5
$2600 ext{-} ext{K-}1.0 ext{-}100 ext{k}$	2.5	8.0	2.6
$2600 ext{-} ext{K-}5.0 ext{-}60 ext{k}$	7.4	23.9	7.9
$2600\text{-}\mathrm{K}\text{-}5.0\text{-}80\mathrm{k}$	5.7	18.3	6.1
$2600 ext{-} ext{K-}5.0 ext{-}100 ext{k}$	4.8	15.4	5.1
$2600\text{-}\mathrm{K}\text{-}10.0\text{-}60\mathrm{k}$	13.7	42.5	14.6
$2600\text{-}\mathrm{K}\text{-}10.0\text{-}80\mathrm{k}$	11.3	35.1	12.1
$2600\text{-}\mathrm{K}\text{-}10.0\text{-}100\mathrm{k}$	9.9	30.7	10.5

Bibliography

- Adibekyan, V. Z., Sousa, S. G., Santos, N. C., Mena, E. D., Hernández, J. I. G., Israelian, G., Mayor, M., and Khachatryan, G.: 2012, Astronomy and Astrophysics 545, A32
- Allard, F.: 2013, Proceedings of the International Astronomical Union 8(S299), 271, 00007
- Allard, F., Homeier, D., and Freytag, B.: 2010, arXiv:1011.5405 [astro-ph], 00066
- Andreasen, D. T., Sousa, S. G., Delgado Mena, E., Santos, N. C., Tsantaki, M., Rojas-Ayala, B., and Neves, V.: 2016, Astronomy and Astrophysics 585, A143
- Artigau, E., Kouach, D., Donati, J.-F., Doyon, R., Delfosse, X., Baratchart, S., Lacombe, M., Moutou, C., Rabou, P., Parès, L. P., Micheau, Y., Thibault, S., Reshetov, V. A., Dubois, B., Hernandez, O., Vallée, P., Wang, S.-Y., Dolon, F., Pepe, F. A., Bouchy, F., Striebig, N., Hénault, F., Loop, D., Saddlemyer, L., Barrick, G., Vermeulen, T., Dupieux, M., Hébrard, G., Boisse, I., Martioli, E., Alencar, S. H. P., do Nascimento, J.-D., and Figueira, P.: 2014, in *Proc.SPIE*, Vol. 9147, p. 914715, International Society for Optics and Photonics, 00047
- Artigau, E., Malo, L., Doyon, R., Figueira, P., Delfosse, X., and Astudillo-Defru, N.: 2018, *The Astronomical Journal* 155, 198
- Asplund, M., Grevesse, N., Sauval, A. J., and Scott, P.: 2009, Annual Review of Astronomy and Astrophysics 47, 481
- Astudillo-Defru, N., Bonfils, X., Delfosse, X., Ségransan, D., Forveille, T., Bouchy, F., Gillon, M., Lovis, C., Mayor, M., Neves, V., Pepe, F., Perrier, C., Queloz, D., Rojo, P., Santos, N. C., and Udry, S.: 2015, Astronomy and Astrophysics 575, A119
- Baraffe, I., Chabrier, G., Barman, T., Allard, F., and Hauschildt, P. H.: 2003, Astronomy and Astrophysics 402(2), 701, 00000
- Baraffe, I., Homeier, D., Allard, F., and Chabrier, G.: 2015, Astronomy and Astrophysics 577, A42, 00280
- Barnes, J. R., Barman, T. S., Jones, H. R. A., Leigh, C. J., Cameron, A. C., Barber, R. J., and Pinfield, D. J.: 2008, Monthly Notices of the Royal Astronomical Society 390(3), 1258

Barros, S. C. C., Gosselin, H., Lillo-Box, J., Bayliss, D., Mena, E. D., Brugger, B., Santerne, A., Armstrong, D. J., Adibekyan, V., Armstrong, J. D., Barrado, D., Bento, J., Boisse, I., Bonomo, A. S., Bouchy, F., Brown, D. J. A., Cochran, W. D., Cameron, A. C., Deleuil, M., Demangeon, O., Díaz, R. F., Doyle, A., Dumusque, X., Ehrenreich, D., Espinoza, N., Faedi, F., Faria, J. P., Figueira, P., Foxell, E., Hébrard, G., Hojjatpanah, S., Jackman, J., Lendl, M., Ligi, R., Lovis, C., Melo, C., Mousis, O., Neal, J. J., Osborn, H. P., Pollacco, D., Santos, N. C., Sefako, R., Shporer, A., Sousa, S. G., Triaud, A. H. M. J., Udry, S., Vigan, A., and Wyttenbach, A.: 2017, Astronomy & Astrophysics 608, A25

- Bean, J. L., Miller-Ricci Kempton, E., and Homeier, D.: 2010, Nature 468, 669, 00283
- Benedict, G. F. and Harrison, T. E.: 2017, The Astronomical Journal 153, 258
- Bertaux, J. L., Lallement, R., Ferron, S., Boonne, C., and Bodichon, R.: 2014, Astronomy and Astrophysics 564, A46, 00041
- Bevington, P. R. and Robinson, D. K.: 2003, Data Reduction and Error Analysis for the Physical Sciences, McGraw-Hill, p.g. 208-212
- Birkby, J. L., de Kok, R. J., Brogi, M., Schwarz, H., and Snellen, I. a. G.: 2017, The Astronomical Journal 153(3), 138
- Bonfanti, A., Ortolani, S., and Nascimbeni, V.: 2016, Astronomy and Astrophysics 585, A5
- Bouchy, F., Doyon, R., Artigau, E., Melo, C., Hernandez, O., Wildi, F., Delfosse, X., Lovis, C., Figueira, P., Canto Martins, B. L., González Hernández, J. I., Thibault, S., Reshetov, V., Pepe, F., Santos, N. C., de Medeiros, J. R., Rebolo, R., Abreu, M., Adibekyan, V. Z., Bandy, T., Benz, W., Blind, N., Bohlender, D., Boisse, I., Bovay, S., Broeg, C., Brousseau, D., Cabral, A., Chazelas, B., Cloutier, R., Coelho, J., Conod, U., Cumming, A., Delabre, B., Genolet, L., Hagelberg, J., Jayawardhana, R., Käufl, H.-U., Lafrenière, D., de Castro Leão, I., Malo, L., de Medeiros Martins, A., Matthews, J. M., Metchev, S., Oshagh, M., Ouellet, M., Parro, V. C., Rasilla Piñeiro, J. L., Santos, P., Sarajlic, M., Segovia, A., Sordet, M., Udry, S., Valencia, D., Vallée, P., Venn, K., Wade, G. A., and Saddlemyer, L.: 2017, *The Messenger* 169, 21, 00000
- Bouchy, F., Pepe, F., and Queloz, D.: 2001, Astronomy and Astrophysics 374(2), 733, 00258
- Brogi, M., de Kok, R. J., Albrecht, S., Snellen, I. A. G., Birkby, J. L., and Schwarz, H.: 2016, *The Astrophysical Journal* 817(2), 106, 00000
- Brogi, M., de Kok, R. J., Birkby, J. L., Schwarz, H., and Snellen, I. A. G.: 2014, Astronomy and Astrophysics 565, A124, 00000
- Brogi, M., Snellen, I. A. G., de Kok, R. J., Albrecht, S., Birkby, J., and de Mooij, E. J. W.: 2012, *Nature* 486, 502, 00000
- Burrows, A., Marley, M., Hubbard, W. B., Lunine, J. I., Guillot, T., Saumon, D., Freedman, R., Sudarsky, D., and Sharp, C.: 1997, *The Astrophysical Journal* 491, 856
- Chabrier, G. and Baraffe, I.: 2000, Annual Review of Astronomy and Astrophysics 38(1), 337, 00483
- Chen, J. and Kipping, D. M.: 2016, The Astrophysical Journal 834(1), 17

- Ciddor, P. E.: 1996, Applied Optics **3**5(9), 1566
- Clough, S. A. and Iacono, M. J.: 1995, Journal of Geophysical Research: Atmospheres 100(D8), 16519, 00002
- Collaboration, G., Brown, A. G. A., Vallenari, A., Prusti, T., Bruijne, D., J. H., Babusiaux, C., and Bailer-Jones, C. a. L.: 2018, *ArXiv e-prints* p. arXiv:1804.09365
- Connes, P.: 1985, Astrophysics and Space Science 110(2), 211
- Connes, P., Martic, M., and Schmitt, J.: 1996, Astrophysics and Space Science 241(1), 61
- Correia, A. C. M., Udry, S., Mayor, M., Laskar, J., Naef, D., Pepe, F., Queloz, D., and Santos, N. C.: 2005, aap 440, 751, 00000
- Cotton, D. V., Bailey, J., and Kedziora-Chudczer, L.: 2014, Monthly Notices of the Royal Astronomical Society 439, 387, 00007
- Crepp, J. R., Gonzales, E. J., Bechter, E. B., Montet, B. T., Johnson, J. A., Piskorz, D., Howard, A. W., and Isaacson, H.: 2016, *The Astrophysical Journal* 831, 00004
- Czekala, I., Andrews, S. M., Mandel, K. S., Hogg, D. W., and Green, G. M.: 2015, The Astrophysical Journal 812(2), 128, 00022
- Czesla, S., Molle, T., and Schmitt, J. H. M. M.: 2018, Astronomy and Astrophysics 609, A39
- de Kok, R. J., Brogi, M., Snellen, I. A., Birkby, J., Albrecht, S., and de Mooij, E. J.: 2013, Astronomy and Astrophysics 554, A82, 00086
- Deeg, H.: 1998, in Brown Dwarfs and Extrasolar Planets, Vol. 134 of ASP Conference Series #134, p. 216
- Dorn, R. J., Finger, G., Huster, G., Kaeufl, H.-U., Lizon, J.-L., Mehrgan, L., Meyer, M., Pirard, J.-F., Silber, A., Stegmeier, J., and Moorwood, A. F. M.: 2004, in *Optical and Infrared Detectors for Astronomy*, Vol. 5499, pp 510–518, International Society for Optics and Photonics
- Dorn, R. J., Follert, R., Bristow, P., Cumani, C., Eschbaumer, S., Grunhut, J., Haimerl, A., Hatzes, A., Heiter, U., and Hinterschuster, R.: 2016, in Ground-Based and Airborne Instrumentation for Astronomy VI, Vol. 9908, p. 99080I, International Society for Optics and Photonics, 00002
- Edlén, B.: 1953, JOSA 43(5), 339
- ESO: 2017, ESO Call for Proposals P101
- Ferluga, S., Floreano, L., Bravar, U., and Bédalo, C.: 1997, Astronomy and Astrophysics Supplement Series 121(1), 201, 00012
- Figueira, P., Adibekyan, V. Z., Oshagh, M., Neal, J. J., Rojas-Ayala, B., Lovis, C., Melo, C., Pepe, F., Santos, N. C., and Tsantaki, M.: 2016, Astronomy and Astrophysics 586, A101, 00002
- Figueira, P. and Neves, S.: 2015, Astro Homus, CAUP

Figueira, P., Pepe, F., Melo, C. H. F., Santos, N. C., Lovis, C., Mayor, M., Queloz, D., Smette, A., and Udry, S.: 2010, Astronomy and Astrophysics 511, A55, 00057

- Freudling, W., Romaniello, M., Bramich, D. M., Ballester, P., Forchi, V., García-Dabló, C. E., Moehler, S., and Neeser, M. J.: 2013, Astronomy and Astrophysics 559, A96
- Gray, D. F.: 2005, *The Observation and Analysis of Stellar Photospheres*, Cambridge University Press, 3 edition
- Gullikson, K., Dodson-Robinson, S., and Kraus, A.: 2014, The Astronomical Journal 148(3), 53, 00015
- Hadrava, P.: 2009, arXiv:0909.0172 [astro-ph], 00013
- Halbwachs, J.-L., Arenou, F., Mayor, M., Udry, S., and Queloz, D.: 2000, Astronomy and Astrophysics 355, 581, 00198
- Hatzes, A. P. and Cochran, W. D.: 1992, Vol. 40, p. 275
- Hatzes, A. P. and Rauer, H.: 2015, The Astrophysical Journal Letters 810, L25
- Hoeijmakers, H. J., Kok, D., J, R., Snellen, I. a. G., Brogi, M., Birkby, J. L., and Schwarz, H.: 2015, Astronomy and Astrophysics 575, A20
- Horne, K.: 1986, Publications of the Astronomical Society of the Pacific 98, 609, 01548
- Husser, T.-O., von Berg, S. W., Dreizler, S., Homeier, D., Reiners, A., Barman, T., and Hauschildt, P. H.: 2013, Astronomy and Astrophysics 553, A6, 00243
- Kaeufl, H.-U., Ballester, P., Biereichel, P., Delabre, B., Donaldson, R., Dorn, R., Fedrigo, E., Finger, G., Fischer, G., Franza, F., Gojak, D., Huster, G., Jung, Y., Lizon, J.-L., Mehrgan, L., Meyer, M., Moorwood, A., Pirard, J.-F., Paufique, J., Pozna, E., Siebenmorgen, R., Silber, A., Stegmeier, J., and Wegerer, S.: 2004, Ground-based Instrumentation for Astronomy 5492, 1218, 00000
- Kerber, F., Nave, G., Sansonetti, C. J., and Bristow, P.: 2009, Physica Scripta 2009(T134), 014007, 00009
- Kolbl, R., Marcy, G. W., Isaacson, H., and Howard, A. W.: 2015, The Astronomical Journal 149, 18
- Kostogryz, N., Kürster, M., Yakobchuk, T., Lyubchik, Y., and Kuznetsov, M.: 2013, Astronomische Nachrichten 334(7), 648, 00000
- Ku, H. H.: 1966, Notes on the Use of Propagation of Error Formulas, National Bureau of Standards
- Lillo-Box, J., Leleu, A., Parviainen, H., Figueira, P., Mallonn, M., Correia, A. C. M., Santos, N. C., Robutel, P., Lendl, M., Boffin, H. M. J., Faria, J. P., Barrado, D., and Neal, J.: 2018, arXiv:1807.00773 [astro-ph]
- Maldonado, J. and Villaver, E.: 2017, Astronomy and Astrophysics 602, A38
- Martins, J. H. C., Santos, N. C., Figueira, P., Faria, J. P., Montalto, M., Boisse, I., Ehrenreich, D., Lovis, C., Mayor, M., Melo, C., Pepe, F., Sousa, S. G., Udry, S., and Cunha, D.: 2015, Astronomy and Astrophysics 576, A134

- Mathar, R. J.: 2007, Journal of Optics A: Pure and Applied Optics 9(5), 470
- Mayor, M. and Queloz, D.: 1995, Nature 378(6555), 355
- Meier, R. J.: 2005, Vibrational Spectroscopy 39(2), 266
- Moutou, C., Vigan, A., Mesa, D., Desidera, S., Thébault, P., Zurlo, A., and Salter, G.: 2017, Astronomy and Astrophysics 602, A87, 00001
- Murray, C. D. and Correia, A. C. M.: 2010, in S. Seager (ed.), *Exoplanets*, pp 15–23, University of Arizona Press, 00000
- Nemravová, J. A., Harmanec, P., Brož, M., Vokrouhlický, D., Mourard, D., Hummel, C. A., Cameron, C., Matthews, J. M., Bolton, C. T., Božić, H., Chini, R., Dembsky, T., Engle, S., Farrington, C., Grunhut, J. H., Guenther, D. B., Guinan, E. F., Korčáková, D., Koubský, P., Kříček, R., Kuschnig, R., Mayer, P., McCook, G. P., Moffat, A. F. J., Nardetto, N., Prša, A., Ribeiro, J., Rowe, J., Rucinski, S., Škoda, P., Šlechta, M., Tallon-Bosc, I., Votruba, V., Weiss, W. W., Wolf, M., Zasche, P., and Zavala, R. T.: 2016, Astronomy and Astrophysics 594, A55
- Nicholls, C. P., Lebzelter, T., Smette, A., Wolff, B., Hartman, H., Käufl, H.-U., Przybilla, N., Ramsay, S., Uttenthaler, S., Wahlgren, G. M., and others: 2017, Astronomy and Astrophysics 598, A79, 00000
- Passegger, V. M., Berg, S. W.-v., and Reiners, A.: 2016, Astronomy and Astrophysics 587, A19, 00006
- Peck, E. R. and Reeder, K.: 1972, JOSA 62(8), 958
- Pilyavsky, G., Mahadevan, S., Kane, S. R., Howard, A. W., Ciardi, D. R., de Pree, C., Dragomir, D., Fischer, D., Henry, G. W., Jensen, E. L. N., Laughlin, G., Marlowe, H., Rabus, M., von Braun, K., Wright, J. T., and Wang, X. X.: 2011, apj 743, 162, 00014
- Piskorz, D., Benneke, B., Crockett, N. R., Lockwood, A. C., Blake, G. A., Barman, T. S., Bender, C. F., Bryan, M. L., Carr, J. S., Fischer, D. A., Howard, A. W., Isaacson, H., and Johnson, J. A.: 2016, *The Astrophysical Journal* 832(2), 131
- Piskunov, N. E. and Valenti, J. A.: 2002, Astronomy and Astrophysics 385(3), 1095, 00257
- Quarteroni, A., Sacco, R., and Saleri, F.: 2000, *Numerical Mathematics*, No. 37 in Texts in applied mathematics, Springer, New York
- Quirrenbach, A., Amado, P. J., Caballero, J. A., Mundt, R., Reiners, A., Ribas, I., Seifert, W., Abril, M., Aceituno, J., Alonso-Floriano, F. J., Ammler-von Eiff, M., Antona Jiménez, R., Anwand-Heerwart, H., Azzaro, M., Bauer, F., Barrado, D., Becerril, S., Béjar, V. J. S., Benítez, D., Berdiñas, Z. M., Cárdenas, M. C., Casal, E., Claret, A., Colomé, J., Cortés-Contreras, M., Czesla, S., Doellinger, M., Dreizler, S., Feiz, C., Fernández, M., Galadí, D., Gálvez-Ortiz, M. C., García-Piquer, A., García-Vargas, M. L., Garrido, R., Gesa, L., Gómez Galera, V., González Álvarez, E., González Hernández, J. I., Grözinger, U., Guàrdia, J., Guenther, E. W., de Guindos, E., Gutiérrez-Soto, J., Hagen, H.-J., Hatzes, A. P., Hauschildt, P. H., Helmling, J., Henning, T., Hermann, D., Hernández Castaño, L., Herrero, E., Hidalgo, D., Holgado, G., Huber, A., Huber, K. F., Jeffers, S., Joergens, V., de Juan, E., Kehr, M., Klein, R., Kürster, M., Lamert, A., Lalitha, S., Laun, W., Lemke, U., Lenzen, R., López del Fresno, M., López Martí, B., López-Santiago, J., Mall, U., Mandel, H., Martín, E. L., Martín-Ruiz, S.,

Martínez-Rodríguez, H., Marvin, C. J., Mathar, R. J., Mirabet, E., Montes, D., Morales Muñoz, R., Moya, A., Naranjo, V., Ofir, A., Oreiro, R., Pallé, E., Panduro, J., Passegger, V.-M., Pérez-Calpena, A., Pérez Medialdea, D., Perger, M., Pluto, M., Ramón, A., Rebolo, R., Redondo, P., Reffert, S., Reinhardt, S., Rhode, P., Rix, H.-W., Rodler, F., Rodríguez, E., Rodríguez-López, C., Rodríguez-Pérez, E., Rohloff, R.-R., Rosich, A., Sánchez-Blanco, E., Sánchez Carrasco, M. A., Sanz-Forcada, J., Sarmiento, L. F., Schäfer, S., Schiller, J., Schmidt, C., Schmitt, J. H. M. M., Solano, E., Stahl, O., Storz, C., Stürmer, J., Suárez, J. C., Ulbrich, R. G., Veredas, G., Wagner, K., Winkler, J., Zapatero Osorio, M. R., Zechmeister, M., Abellán de Paco, F. J., Anglada-Escudé, G., del Burgo, C., Klutsch, A., Lizon, J. L., López-Morales, M., Morales, J. C., Perryman, M. A. C., Tulloch, S. M., and Xu, W.: 2014, in *Prococeedings of SPIE: Ground-Based and Airborne Instrumentation for Astronomy V*, Vol. 9147, p. 91471F

- Rodler, F., Lopez-Morales, M., and Ribas, I.: 2012, The Astrophysical Journal Letters 753(1), L25, 00077
- Rothman, L., Gordon, I., Babikov, Y., Barbe, A., Chris Benner, D., Bernath, P., Birk, M., Bizzocchi, L., Boudon, V., Brown, L., Campargue, A., Chance, K., Cohen, E., Coudert, L., Devi, V., Drouin, B., Fayt, A., Flaud, J.-M., Gamache, R., Harrison, J., Hartmann, J.-M., Hill, C., Hodges, J., Jacquemart, D., Jolly, A., Lamouroux, J., Le Roy, R., Li, G., Long, D., Lyulin, O., Mackie, C., Massie, S., Mikhailenko, S., Müller, H., Naumenko, O., Nikitin, A., Orphal, J., Perevalov, V., Perrin, A., Polovtseva, E., Richard, C., Smith, M., Starikova, E., Sung, K., Tashkun, S., Tennyson, J., Toon, G., Tyuterev, V., and Wagner, G.: 2013, Journal of Quantitative Spectroscopy and Radiative Transfer 130, 4, 01706
- Rothman, L., Gordon, I., Barbe, A., Benner, D., Bernath, P., Birk, M., Boudon, V., Brown, L., Campargue, A., Champion, J.-P., Chance, K., Coudert, L., Dana, V., Devi, V., Fally, S., Flaud, J.-M., Gamache, R., Goldman, A., Jacquemart, D., Kleiner, I., Lacome, N., Lafferty, W., Mandin, J.-Y., Massie, S., Mikhailenko, S., Miller, C., Moazzen-Ahmadi, N., Naumenko, O., Nikitin, A., Orphal, J., Perevalov, V., Perrin, A., Predoi-Cross, A., Rinsland, C., Rotger, M., Šimečková, M., Smith, M., Sung, K., Tashkun, S., Tennyson, J., Toth, R., Vandaele, A., and Vander Auwera, J.: 2009, Journal of Quantitative Spectroscopy and Radiative Transfer 110(9-10), 533, 00000
- Sahlmann, J., Segransan, D., Queloz, D., Udry, S., Santos, N. C., Marmier, M., Mayor, M., Naef, D., Pepe, F., and Zucker, S.: 2011, Astronomy and Astrophysics 525, A95, 00115
- Santerne, A., Brugger, B., Armstrong, D. J., Adibekyan, V., Lillo-Box, J., Gosselin, H., Aguichine, A., Almenara, J.-M., Barrado, D., Barros, S. C. C., Bayliss, D., Boisse, I., Bonomo, A. S., Bouchy, F., Brown, D. J. A., Deleuil, M., Mena, E. D., Demangeon, O., Díaz, R. F., Doyle, A., Dumusque, X., Faedi, F., Faria, J. P., Figueira, P., Foxell, E., Giles, H., Hébrard, G., Hojjatpanah, S., Hobson, M., Jackman, J., King, G., Kirk, J., Lam, K. W. F., Ligi, R., Lovis, C., Louden, T., McCormac, J., Mousis, O., Neal, J. J., Osborn, H. P., Pepe, F., Pollacco, D., Santos, N. C., Sousa, S. G., Udry, S., and Vigan, A.: 2018, Nature Astronomy 2(5), 393
- Santerne, A., Díaz, R. F., Moutou, C., Bouchy, F., Hébrard, G., Almenara, J.-M., Bonomo, A. S., Deleuil, M., and Santos, N. C.: 2012, Astronomy and Astrophysics 545, A76
- Santos, N. C., Adibekyan, V., Figueira, P., Andreasen, D. T., Barros, S. C. C., Delgado-Mena, E., Demangeon, O., Faria, J. P., Oshagh, M., Sousa, S. G., Viana, P. T. P., and Ferreira, A. C. S.: 2017, Astronomy and Astrophysics 603, A30, 00001

- Santos, N. C., Israelian, G., and Mayor, M.: 2004, aap 415, 1153, 00000
- Santos, N. C., Israelian, G., Mayor, M., Bento, J. P., Almeida, P. C., Sousa, S. G., and Ecuvillon, A.: 2005, aap 437, 1127, 00000
- Schlaufman, K. C.: 2018, The Astrophysical Journal 853, 37
- Schwarz, G.: 1978, The Annals of Statistics 6(2), 461
- Seifahrt, A., Käufl, H. U., Zängl, G., Bean, J. L., Richter, M. J., and Siebenmorgen, R.: 2010, Astronomy and Astrophysics 524, A11
- Skrutskie, M. F., Cutri, R. M., Stiening, R., Weinberg, M. D., Schneider, S., Carpenter, J. M., Beichman, C., Capps, R., Chester, T., Elias, J., Huchra, J., Liebert, J., Lonsdale, C., Monet, D. G., Price, S., Seitzer, P., Jarrett, T., Kirkpatrick, J. D., Gizis, J. E., Howard, E., Evans, T., Fowler, J., Fullmer, L., Hurt, R., Light, R., Kopan, E. L., Marsh, K. A., McCallon, H. L., Tam, R., Van Dyk, S., and Wheelock, S.: 2006, *The Astronomical Journal* 131, 1163
- Smette, A., Sana, H., Noll, S., Horst, H., Kausch, W., Kimeswenger, S., Barden, M., Szyszka, C., Jones, A. M., Gallenne, A., Vinther, J., Ballester, P., and Taylor, J.: 2015, Astronomy and Astrophysics 576, A77, 00067
- Snellen, I. A. G., Brandl, B. R., Kok, D., J, R., Brogi, M., Birkby, J., and Schwarz, H.: 2014, *Nature* 509, 63, 00000
- Snellen, I. A. G., Kok, D., J. R., Mooij, D., W. E. J., and Albrecht, S.: 2010, Nature 465(7301), 1049
- Soderblom, D. R.: 2010, Annual Review of Astronomy and Astrophysics 48, 581, 00241
- Sorahana, S., Yamamura, I., and Murakami, H.: 2013, The Astrophysical Journal 767(1), 77
- Sousa, S. G., Santos, N. C., Mayor, M., Udry, S., Casagrande, L., Israelian, G., Pepe, F., Queloz, D., and Monteiro, M. J. P. F. G.: 2008, aap 487, 373, 00390
- Tody, D.: 1993, in R. J. Hanisch, R. J. V. Brissenden, and J. Barnes (eds.), Astronomical Data Analysis Software and Systems II, Vol. 52 of Astronomical Society of the Pacific Conference Series, p. 173, 00000
- Tsantaki, M., Sousa, S. G., Adibekyan, V. Z., Santos, N. C., Mortier, A., and Israelian, G.: 2013, *aap* **5**55, A150, 00077
- Udry, S., Mayor, M., Naef, D., Pepe, F., Queloz, D., Santos, N. C., and Burnet, M.: 2002, Astronomy and Astrophysics 390(1), 267, 00158
- Ulmer-Moll, S., Figueira, P., Neal, J. J., Santos, N. C., and Bonnefoy, M.: 2018, Astronomy and Astrophysics, in review
- Vacca, W. D., Cushing, M. C., and Rayner, J. T.: 2003, Publications of the Astronomical Society of the Pacific 115(805), 389, 00000
- Wenger, M., Ochsenbein, F., Egret, D., Dubois, P., Bonnarel, F., Borde, S., Genova, F., Jasniewicz, G., Laloë, S., Lesteven, S., and Monier, R.: 2000, Astronomy and Astrophysics Supplement Series 143, 9

Whitworth, A., Bate, M. R., Nordlund, A., Reipurth, B., and Zinnecker, H.: 2007, *Protostars and Planets* V pp 459–476, 00087

Zechmeister, M., Reiners, A., Amado, P. J., Azzaro, M., Bauer, F. F., Béjar, V. J. S., Caballero, J. A., Guenther, E. W., Hagen, H.-J., Jeffers, S. V., Kaminski, A., Kürster, M., Launhardt, R., Montes, D., Morales, J. C., Quirrenbach, A., Reffert, S., Ribas, I., Seifert, W., Tal-Or, L., and Wolthoff, V.: 2018, Astronomy and Astrophysics 609, A12

Zucker, S. and Mazeh, T.: 2001, The Astrophysical Journal 562(1), 549, 00060